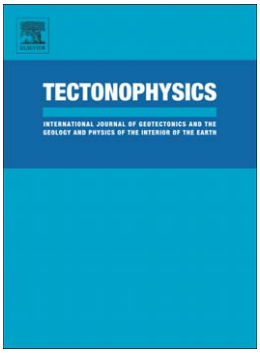

Slip-rates of blind thrusts in slow deforming areas: examples from the Po Plain (Italy)

Francesco Emanuele Maesano, Chiara D'Ambrogi, Pierfrancesco Burrato, Giovanni Toscani

PII: S0040-1951(14)00644-1
DOI: doi: 10.1016/j.tecto.2014.12.007
Reference: TECTO 126498

To appear in: *Tectonophysics*

Received date: 22 September 2014
Revised date: 26 November 2014
Accepted date: 23 December 2014

Please cite this article as: Maesano, Francesco Emanuele, D'Ambrogi, Chiara, Burrato, Pierfrancesco, Toscani, Giovanni, Slip-rates of blind thrusts in slow deforming areas: examples from the Po Plain (Italy), *Tectonophysics* (2015), doi: 10.1016/j.tecto.2014.12.007

Slip-rates of blind thrusts in slow deforming areas: examples from the Po Plain (Italy)

Francesco Emanuele Maesano[1], Chiara D'Ambrogi[2], Pierfrancesco Burrato[3], Giovanni Toscani[4]

[1]Consultant at ISPRA Servizio Geologico d'Italia, Via Vitaliano Brancati, 48, 00144 Roma, Italy

[2]ISPRA Servizio Geologico d'Italia, Via Vitaliano Brancati, 48, 00144 Roma, Italy

[3]Istituto Nazionale di Geofisica e Vulcanologia, Via di Vigna Murata, 605 - 00143 Roma, Italy

[4]Dipartimento di Scienze della Terra e dell'Ambiente, Università di Pavia, Via Ferrata, 1 - 27100 Pavia, Italy

Corresponding Author:

Pierfrancesco Burrato

Istituto Nazionale di Geofisica e Vulcanologia

Via di Vigna Murata, 605

00143 - Roma, Italy

Tel.: ++39-06-51860492

Fax: ++39-06-51860507

E-mail: pierfrancesco.burrato@ingv.it

Running title: Slip rates in the Po Plain

Abstract

We calculate Plio-Pleistocene slip rates on the blind thrusts of the outer Northern Apennines fronts, that are the potential sources of highly damaging earthquakes, as shown by the M_W 6.1-6.0, 2012 Emilia-Romagna seismic sequence. Slip rates are a key parameter for understanding the seismogenic potential of active fault systems and assessing the seismic hazard they pose, however, they are difficult to calculate in slow deforming areas like the Po Plain where faulting and folding is mostly blind. To overcome this, we developed a workflow which included the preparation of a homogeneous regional dataset of geological and geophysical subsurface information, rich in Plio-Pleistocene data. We then constructed 3D geological models around selected individual structures to decompact the clastic units and restore the slip on the fault planes. The back-stripping of the differential compaction eliminates unwanted overestimation of the slip rates due to compaction-induced differential subsidence. Finally, to restore the displacement we used different methods according to the deformation style, i.e. Fault Parallel Flow for faulted horizons, trishear and elastic dislocation modeling for fault-propagation folds. The result of our study is the compilation of a slip rate database integrating former published values with 28 new values covering a time interval from the Pliocene to the present. It contains data on 14 individual blind thrusts including the Mirandola thrust, seismogenic source of the 29 May 2012, M_W 6.0 earthquake. Our study highlights that the investigated thrusts were active with rates ranging between 0.1-1.0 mm/yr during the last 1.81 Myr. The Mirandola thrust slipped at 0.86±0.38 mm/yr during the last 0.4 Myr. These rates calculated with an homogeneous methodology through the entire Po Plain can be charged entirely to the thrust activity and not to secondary effects like the differential compaction of sediments across the structures.

Keywords: blind thrusts; slip rates; 3D geological modeling; sediment decompaction; Po Plain; Northern Apennines

1. Introduction

The Po Plain stretches for over 400 km in a roughly east-west direction from the Western Alps to the Adriatic Sea, extending for over 15% of the national territory and comprising the largest alluvial plain of Italy. Geologically the Po Plain comprises the foreland area of the two active, oppositely-verging fold-and-thrust belts: the Northern Apennines (hereinafter also NA), to the south, and the Southern Alps (hereinafter also SA), to the north and to the west. Their uplifted, tightly folded and intensely eroded accretionary wedges encircle the Po Plain in all directions but to the east, marking its morphological boundaries. The outer deformation fronts of the two belts are currently buried below the thick Pliocene-Quaternary, marine to continental succession that fills-in the Po Plain; for this reason the surface evidence of the ongoing activity of the thrusts of the two belts is restricted to their exposed margins and to a few isolated spots in the plain proper. GPS data document active shortening across the NA and SA fronts with velocities up to 2.5 mm/yr (e.g. Devoti et al., 2011; Michetti et al., 2012). A fraction of this strain is released by moderate yet damaging earthquakes such as the recent 20 and 29 May 2012, M_W 6.1-6.0, Emilia events, generated by blind thrusts of the outermost front of the Northern Apennines (Anzidei et al., 2012; Govoni et al., 2014).

Earthquake activity in flat alluvial plains poses an especially insidious threat as most of the population and the largest industrial facilities normally take advantage of these gentle landscapes. The Po Plain does not escape this general rule as it hosts nearly a third of Italy's population along with important historical centers, many industrial facilities and lots of critical infrastructures. Even though on average the seismic hazard of the Po Plain is comparatively low (MPS04 Working Group, 2004), the 2012 earthquakes demonstrated that locally it may be rather high and comparable to the most earthquake-prone areas of Italy. In combination with the high exposure and vulnerability to earthquakes of most of the Po Plain, also its seismic risk may be locally very high. Once again this circumstance was tragically revealed by the 2012 earthquakes, that shattered a crucial industrial district causing a loss of about 2% in Italy's GNP despite their limited size.

The 2012 earthquakes definitely raised awareness of the risk posed by the numerous blind thrusts buried beneath the Po Plain; but while assessing the region's exposure and vulnerability is relatively straightforward, little is known to date about how tectonic strain is partitioned across the different faults, that is to say, about their slip rates. This information is crucial for ranking the different active portions of the Po Plain and describing the spatial variability of seismic hazard, and hence of seismic risk.

Dealing with blind thrusts is not easy nor straightforward, however, which partially explains why the seismogenic potential of Po Plain faults has gone unappreciated for so long. When blind faulting occurs in flat terrains like the Po Plain the associated hazard is generally not perceived by the population and by the decision makers – and sometimes even by scientists - due to the lack of associated morphologies. In fact, in most earthquake-prone areas worldwide the hazard posed by hidden and blind faults has been clearly recognized only after the publication of the seminal paper of Stein and Yeats (1989) based on their pioneering work in California. But compared to California strain rates, the low rates that are typical of the Po Plain result in long earthquake return times, further stressing the perception of a low local hazard. For the same reasons and for the inherent difficulty in identifying the hidden or blind seismogenic sources and characterize their seismic behavior, the hazard they pose is also difficult to assess using traditional geologic tools. Recent worldwide examples of earthquakes that were caused by blind, hard-to-identify or previously unmapped faults show that this issue is critical even in countries where active faulting studies are especially advanced, though mostly focused on surface cutting structures. The 25 March 2007, M_w 6.9, Noto-Hanto, Japan (Toda and Awata, 2008), the 4 September 2010, M_w 7.1, Canterbury, New Zealand (Quigley et al., 2010), and the 23 October 2011, M_w 7.1, Van, eastern Turkey earthquakes are examples of events that occurred on unidentified seismogenic sources and were hence largely unexpected.

In this work we focused on the compressional structures of the outer Northern Apennines thrust fronts and calculated slip rates for several blind thrusts of this buried mountain belt. To this

end we used a compilation of geophysical and stratigraphic subsurface data from various sources, merged into a homogenized regional 3D dataset and analyzed with standardized procedures. We followed the approach discussed by Maesano et al. (2013) to quantify the active deformation of the Emilia and Ferrara-Romagna arcs of the Northern Apennines outer buried thrust fronts using a regional dataset of homogenized geological cross-sections and a few selected Pliocene-Quaternary chronostratigraphic horizons covering the southern part of the Po Plain (i.e. to the south of the Po River). From this dataset we constructed a regional 3D geological model from which we extracted four regional geological sections and seven shallow sections of local extent, all of which were used in subsequent calculations. The procedure we used to calculate the slip rates of the buried thrust faults included i) the definition of the sedimentary and structural architecture, ii) the decompaction of clastic units, where needed, and iii) the restoration of slip on the fault planes.

The calculation of the slip rate of individual faults may be based on different methodological approaches at different space and time scales: geomorphic and geologic marker analysis (e.g. Ponza et al., 2010), restoration of seismic exploration data (e.g. Maesano et al., 2013), geodetic leveling and GPS observations (e.g. D'Anastasio et al., 2006), and numerical modeling (Kastelic and Carafa, 2012; Barba et al., 2013). We will discuss case by case what strategy or combination of strategies was adopted, depending on the availability of data and on the characteristics of each specific fault.

The main result of our study is the compilation of a database which integrates previously published values with 28 new estimates of slip rate. Our dataset spans the time interval from Pliocene to the Present, constraining the recent activity of the outer Northern Apennines thrust fronts in an unprecedented detail; it contains data concerning 14 individual blind thrusts, including the seismogenic source of the 29 May 2012, M_W 6.0 earthquake. This database can be integrated into seismogenic source models like the DISS seismogenic source database (DISS Working Group, 2010; Basili et al., 2008), thus contributing to future more accurate seismic hazard estimates.

2. Regional geological and tectonic setting

The Northern Apennines are a folded mountain chain that exhibits north-northeastward vergence and convexity (Figure 1), generated starting in the Eocene by westward subduction of the Adriatic lithosphere in the framework of the Africa-Europe plate convergence (for a review see Carminati and Doglioni, 2012, and references therein). The NA are composed of i) a buried depositional wedge covered by the Plio-Quaternary sediments of the Po basin, which started to deform by thrust propagation during the late Messinian-Early Pliocene (Ghielmi et al., 2010; 2013), and ii) an exposed erosional wedge cropping out in the Apennines region proper. Activity of the NA fronts currently concentrates either along blind thrusts buried beneath the Po Plain, or along the partially exposed structures forming the mountain front that bounds the plain to the southwest.

In the absence of direct surface evidence, the buried compressional structures of the Po basin have been extensively investigated for hydrocarbon exploration by means of industrial seismic lines and deep well logs (e.g. Fantoni and Franciosi, 2010; Ghielmi et al., 2010, and references therein). These data revealed a system of N to NE-verging blind thrusts organized in three main folded arcs, which from west to east are: (i) the Monferrato arc, that underwent the smallest amount of shortening and was not considered in this study; (ii) the Emilia arc, that started deforming in the Tortonian and experienced its maximum activity in Piacenzian-Gelasian times; and (iii) the Ferrara-Romagna arc, active since the Messinian (Ghielmi et al., 2013). The structural evolution of the outer NA arcs was not simultaneous across the whole Po Plain: while the Emilia arc reached its present-day configuration in the Zanclean, to the east the outward propagation of the thrust fronts continued until the Zanclean-Piacenzian and the Gelasian, respectively for the inner and for the outer Ferrara arcs (Ghielmi et al., 2010).

At the back of the Emilia and Ferrara-Romagna arcs the sub-emergent Pedeappenninic Thrust Front (PTF, Boccaletti et al., 1985; Bigi et al., 1992) forms the NA mountain front. Its continuing Quaternary activity, although associated with an elusive topographic expression, is recorded by deformation and tilting of river terraces and of exposed syntectonic sediments (Boccaletti et al., 1985 and 2004; Picotti and Pazzaglia, 2008; Wegmann and Pazzaglia, 2009; Ponza et al., 2010).

Conversely, out in the plain there are only few exceptions to the general blind geometry of the buried outer fronts of both the SA and NA chains (Figure 1).

The stratigraphic succession of the Po basin is characterized (from base to top) by a late Paleozoic-Mesozoic evaporitic-silicoclastic and carbonatic sequence deposited on the Adriatic paleomargin and covering the Variscan basement, by Cenozoic deposits of the SA and NA foredeeps, and by Quaternary shallow marine and continental sediments deposited in a generally regressive sequence (Figure 2) (Dondi and D'Andrea, 1986; Bertotti et al., 1993, Argnani and Ricci Lucchi, 2001; Fantoni and Franciosi, 2010; Ghielmi et al., 2010). The structural style of the NA fold-and-thrust belt was governed by the presence of two major detachment levels in the stratigraphic sequence (Figure 2): a deeper one located at the base of the Mesozoic carbonate units within the Triassic evaporites, and a shallower one that can be identified in deposits of upper Oligocene to lower-middle Miocene age, being younger in the eastern part of the Po Plain (e.g. Massoli et al., 2006). The shallow and deep detachments produce structures having shorter and longer wavelength, respectively.

During the Cenozoic compressional cycles the southern part of the Po Plain hosted the foredeep of the NA chain. The associated deposits exhibit a thickness in excess of 8,000 meters and are generally subdivided into five distinct depositional sequences separated by regional unconformities. These unconformities, which date back to the upper Tortonian, upper Messinian, intra Zanclean and Gelasian, can be recognized along the whole Po Plain and Adriatic basins; they have recorded the migration of the foredeep depocenters towards the foreland and the formation of piggy-back basins (Ghielmi et al., 2010).

The shallowest and most recent part of the Po Plain succession (Figure 2 and Table 1) is characterized by a thickness ranging from a few hundred of meters up to 2 km (Castellarin et al., 2006) and is made up of clastic deposits that recorded the last event of marine sedimentation in the basin: they are overlain by Quaternary continental, alluvial and deltaic sediments of the Emiliano-Romagnolo Supersynthem (ERS in Fig. 2) deposited by the Po River and its many tributaries

(Garzanti et al., 2011, and references therein). The prograding deltaic sedimentary wedge is characterized by clinoformal seismic reflectors that exhibit toplap geometry along the NA margin and downlap towards the depocenter (Muttoni et al., 2003; Di Dio et al., 2005; Garzanti et al., 2011; Muttoni et al., 2011). Starting in Gelasian times the deltaic and alluvial sedimentation progressively migrated east-northeastward, causing the infilling of small depocenters located between adjacent structural arcs (Regione Emilia-Romagna and ENI-AGIP, 1998).

2.1. Active deformation and seismicity

GPS data constrain limited ongoing shortening across the Po basin increasing from west to east, with rates ranging between 0.5 and 2.5 mm/yr from the Emilia to the Ferrara thrust fronts (Serpelloni et al., 2005; D'Agostino et al., 2008; Caporali et al., 2011; Devoti et al., 2011; Bennett et al., 2012; Michetti et al., 2012). The observed westward tapering of the convergence documented by GPS goes in parallel with the reduction of the historical and instrumental earthquake moment release (ISIDe Working Group, 2010; Rovida et al., 2011; Vannoli et al., 2014).

Present-day activity of the frontal and outer thrusts of the NA is testified by the historical and instrumental seismicity, the latter characterized by contractional focal mechanisms (Pondrelli et al., 2006; 2011; Figure 1). It is faithfully recorded by faulting and folding of Quaternary alluvial sediments (e.g. Gunderson et al., 2014) and by the influence on the drainage network evolution (e.g. Burrato et al., 2012). Active stress data derived from earthquake focal mechanisms, borehole breakouts and stress orientations measured in young sediments show that the mean orientation of the Sh_{max} is perpendicular to the trend of the buried thrust fronts (Montone and Mariucci, 1999; Heidbach et al., 2010; Montone et al., 2012; Carafa and Barba, 2013), indicating that these compressional structures are favorably oriented with respect to the direction of regional tectonic shortening.

Italian earthquake catalogues show that the Po Plain is the locus of low to moderate seismicity (ISIDe Working Group, 2010; Rovida et al., 2011), yet the area south of the Po River stands out for

larger concentration of events aligned along the eastern Emilia and Ferrara-Romagna arcs and the NA mountain front, the largest being the 5 June 1501, Appennino Modenese earthquake of magnitude 6.0 (Rovida et al., 2011). The most advanced seismogenic source model of the Po basin (DISS: http://diss.rm.ingv.it/diss/), which lists active faults able to generate M 5.5 and larger earthquakes (Basili et al., 2008, DISS Working Group, 2010; Vannoli et al., 2014), includes both the inner (PTF) and the outer (Emilia and Ferrara-Romagna arcs) NA thrust fronts.

This general seismological framework has been recently confirmed by the occurrence of two M_W 6.1 and 6.0 earthquakes on 20 and 29 May 2012 (M_W from Pondrelli et al., 2012) and their aftershock sequence (ISIDe Working Group, 2010; Anzidei et al., 2012; Govoni et al., 2014), that struck the central Po basin about 40 km north-northwest of Bologna. The earthquakes were caused by pure compressional slip over some of the blind thrusts of the western Ferrara-Romagna Arc (see for example Scognamiglio et al., 2012, among several others), thereby activating a 50 km-long stretch of this NA buried outer front and possibly highlighting a stress triggering mechanism among the different activated faults (Bonini et al., 2014). Most of the earthquake sequence was confined between 1 and 12 km depth above the local S-dipping basal detachment of the NA outer thrust front (Govoni et al., 2014). The ongoing activity of these thrusts, also detailed in our study, was first constrained using a combination of geomorphic and subsurface geological data (Burrato et al., 2003, 2012). The Ferrara and Mirandola thrusts of the Ferrara arc are considered to have caused significant drainage diversions of the Po and its main southern tributaries. The coseismic uplift of the ground surface caused by the two mainshocks was recorded with great accuracy by SAR interferometry (Bignami et al., 2012; Pezzo et al., 2013) and was seen to be consistent with the pattern of these drainage anomalies (Burrato et al., 2012).

3. Geological and seismic dataset

The Emilia and Ferrara-Romagna arcs comprise the core of the main Italian hydrocarbon province (e.g. Lindquist, 1999) and are two of the best studied subsurface geological settings of the

entire country. Seismic surveys and borehole drillings performed by oil companies over the past 60 years form the core of a number of published regional sections, such as those recently revised by Fantoni and Franciosi (2010).

We collected most of the published sections crossing the Po Plain, integrating and homogenizing them in a 3D dataset (Figure 3) that was complemented with: i) deep borehole logs (UNMIG: http://sgi.isprambiente.it/geoportal/catalog/content/project/sondaggi.page); ii) contours of the base of Pliocene deposits (Bigi et al., 1992); iii) uninterpreted seismic lines from the ViDEPI database (http://unmig.sviluppoeconomico.gov.it/videpi/en/), and iv) shallow subsurface geological data (Regione Emilia-Romagna and ENI-AGIP, 1998; Regione Lombardia and ENI-AGIP, 2002). We further integrated this dataset with v) the subsurface database of the new Geological Map of Italy at the 1:50,000 scale (http://sgi.isprambiente.it/geoportal/catalog/main/home.page), and with vi) shallow stratigraphies and new chronological data of the Geognostic Database of Regione Emilia-Romagna (available from: http://geo.regione.emilia-romagna.it/sezioni_geo/viewer.htm) derived from continuous core drillings. New stratigraphic age models and chronological constraints for the Po Plain were recently proposed by Gunderson et al. (2014), Muttoni et al. (2003, 2011). They are based on biostratigraphy, magnetostratigraphy, cosmogenic radionuclides burial datings, optically stimulated luminescence datings, and are used here to refine the age of Pleistocene-Holocene horizons.

Starting from this dataset we built a regional geological model of the subsurface of the Po Plain, from which we derived 3D models of key stratigraphic horizons (Figures 4 and 5) and extracted the data along sections that better describe the architecture and deformation history of the Emilia and Ferrara-Romagna arcs. Specifically we used four regional sections that follow those published by Toscani et al. (2006) and by Fantoni and Franciosi (2010) (the traces are shown in Figure 3 and the cross sections are in Figure 6), plus seven shallow sections (traces in Figure 3 and cross sections in Figure 7). All our calculations were based on the following key stratigraphic horizons (Table 1):

- top Messinian (5.33 Myr) (Figure 4);
- top Zanclean (3.60 Myr);
- top Piacenzian (2.59 Myr);
- top Gelasian (1.81 Myr);
- base of the Costamezzana synthem (CMZs, 1.0 Myr);
- base of Emiliano-Romagnolo Inferiore synthem (Figure 5) (ERIs, 0.82 Myr);
- base of Emiliano-Romagnolo Superiore synthem (ERSs, 0.40 Myr).

Locally we also defined the basal surface of the Villa Verrucchio (AES7, 0.125 Myr) and Ravenna subsynthems (AES8, 0.015 Myr). The age of the CMZs basal surface (Sabbie di Imola, as defined by various investigators) ranges from 1.07 Myr in the Parma area (Gunderson et al., 2014) to 0.94 Myr in the Forlì area (Muttoni et al., 2011). The age of the basal surface of ERIs ranges from 0.87 Myr (R surface in Muttoni et al., 2003; Scardia et al., 2012) in the western part of the Po basin to 0.78 Myr in the Romagna area (Muttoni et al., 2011). Finally, the age of the basal surface of ERSs ranges from 0.45 to 0.35 Myr.

For what concern the Pliocene-Pleistocene intervals we adopted the substage names and ages that follow the new subdivision of the IUGS (Cohen et al., 2013).

4. Geological cross-sections

The four regional sections prepared in this study (Figures 1 and 6) run across the Emilia (Sections 1 and 2) and the Ferrara-Romagna arcs (Sections 3 and 4). They are characterized by two main detachment horizons, corresponding to the Marne di Gallare Fm. (upper Oligocene to lower-middle Miocene in age, becoming younger in the eastern Po basin) and to the base of the Mesozoic carbonatic succession (within the Triassic evaporites at the bottom of the Dolomia Principale Formation) (Massoli et al., 2006; Toscani et al., 2006). Significant back-thrusting and a reduced dip of the regional monocline (*sensu* Mariotti and Doglioni, 2000) are characteristic features of the Emilia arc as shown in Sections 1 and 2 (Figure 6), which also illustrate the structural relationships

between the NA and SA outer fronts. Conversely, Sections 3 and 4 (Figures 1 and 6) show no significant back-thrusting and a steeper NA monocline. Along these sections the SA outer thrusts are not visible as they are located further to the north. The rocks forming the basement and the Mesozoic carbonate succession shown in the deeper parts of the four sections are displaced by inherited Mesozoic extensional faults. These structural heterogeneities controlled the vertical and lateral depositional geometry of competent and incompetent sediments across the Adria passive paleo-margin, which in its turn controlled the depth of the main detachment horizons and the three-dimensional structural style of the SA and NA thrust belts (Ravaglia et al., 2006).

The seven shallow sections constructed in this study were obtained from the interpretation of seismic lines and from the regional 3D models of the most continuous and detailed stratigraphic horizons encountered in the subsurface of the Po Plain (Figures 4 and 5). We used these sections a) to describe the depositional geometry of the younger syntectonic deposits of Pleistocene-Holocene age (Table 1), and b) to quantify their deformation in relation with the most recent activity of the main buried thrusts as well as of associated secondary faults (Figure 7). The only stratigraphic horizon recognized throughout the Po Plain - and hence common to all sections - is the base of the ERIs synthem (Figure 5). All other stratigraphic horizons (i.e. base of CMZs, ERSs, AES7 and AES8) are discontinuous and were hence plotted only along specific sections. Except for the Parma and Reggio Emilia (PAa, PAb, PAc and RE in Figure 1), all sections intersect the external part of the exposed NA chain and cross the Emilia and Ferrara-Romagna arcs, generally not far from the regional sections. As such the shallow sections often provide a more detailed view of the same structures described by the regional ones, particularly at shallower stratigraphic levels.

5. Working methodology

5.1 Generalities and restoration workflow

Sections 3 and 4 described the comprehensive dataset of subsurface geological information of the Po Plain stored in the Move software (Midland Valley Exploration Ltd.) that we used to

reconstruct the 3D models of the main subsurface horizons. This database is a multiscale geological model that was progressively integrated with the new available data. Starting from this general model we selected the individual structures that were suited for an in-depth study of their tectonic evolution thanks to the local completeness of the dataset. We used the growth strata geometry of the Pleistocene horizons to infer the geometry of the underlying thrusts, derive their slip rates and reconstruct their Pliocene-Quaternary deformation history. We then selected seven ramp anticlines seen in the regional cross sections of Toscani et al. (2006) and Fantoni and Franciosi (2010): T2EF (east and west), T3EF, T5FF, T6FF, T7RF and T9RF (Figure 6). Along the shallow sections (Figure 7) we investigated six additional thrust-related anticlines having a deep detachment and two smaller ones detaching at shallower depth (along the PR section).

The information stored in our dataset was used to build 3D local models around the ramp anticlines, which in turn were used as a starting sets for our restoration workflow; this is similar to that used by Maesano et al. (2013) and is summarized below (Figure 8).

The first step of our workflow involved decompaction of the younger clastic sedimentary units. After decompaction we selected the most appropriate restoration algorithm for faults and folds for each individual structure (Trishear, Fault Parallel Flow) based on the type of deformation observed. Then for each structure we progressively restored the deformation of the key stratigraphic horizons from the youngest to the oldest, and attempted to estimate the age of inception of activity at the site for which the restoration was being performed. The age of inception was defined as the maximum and minimum age of the first stratigraphic interval affected by syn-sedimentary evidence of tectonic activity, e.g. tilted or faulted horizons or evidence for growth strata.

Our second step was the restoration of pre-deformation conditions, i.e. the calculation of the amount of fault slip needed to retro-deform the selected marker to its initial depositional geometry (for marine deposits this generally corresponds to a horizontal datum).

There are different algorithms than can be used to remove the tectonic deformation (trishear, fault parallel flow and dislocation modeling), depending on the type of deformation observed in each structure (Figure 8).

Once the total slip on the fault plane was determined we calculated the average slip rate for the considered time interval. The entire procedure relied on tools provided by Move (Midland Valley Exploration Ltd.), on the FaultFold 4.5.4 software (1998-2003) (Allmendinger, 1998; Zehnder and Allmendinger, 2000) that allows automating the trial and error trishear workflow, and on the Fault Studio software for dislocation modeling (a technical report of version 1.1 is provided by R. Basili, INGV, http://www.earth-prints.org/handle/2122/1039). The regional cross sections derived from published geological profiles were projected onto straight traces close to the original ones but oriented normal to the average strike of the thrusts and folds to be investigated. The shallow sections deriving from the interpretation of publicly available seismic lines were then converted from time to depth using the velocity data published by the ViDEPI project. In particular we used an average velocity of 1800 m/sec for the depth conversion of the shallower horizons (CMZs and ERIs).

For ensuring that the decompaction procedure was comparable for all structures we used the 3D models of shallower horizons where available; in the other cases we extrapolated each horizon laterally in a 10 km-wide 3D cylindrical buffer.

5.2 Section decompaction

The decompaction of sediments is necessary to remove the effects of rock volume change due to porosity reduction through time. This is a natural phenomenon that affects all sedimentary basins and is related to the progressive consolidation of young saturated sediments. It may locally represent the main reason of natural present-day land subsidence (e.g. Teatini et al., 2011), but it can be driven also by human activity (see for example Stramondo et al., 2007, for the Po Plain). The process of decompaction backstrips a layer of sediments from the model and allows the underlying

rocks to vertically decompact as a result of removal of the overburden. The decompaction algorithm is based on an exponentially decaying porosity with increasing depth of sediments and follows the principles described by Sclater and Christie (1980) and Allen and Allen (1990). In our case studies, the Pliocene-Pleistocene interval is represented by siliciclastic foredeep successions that can be assumed homogeneous in terms of original porosity and elastic properties. Similarly to Scrocca et al. (2007), we modeled them as a sediment mixture with an equal proportion of sand and shale.

The effects of decompaction are more evident in syntectonic layers that were subjected to differential load for an extended period of time; they are larger in the depocenters (syncline axes), where the sedimentary load is greater, than in the structural culminations (anticline axes). Therefore, not considering decompaction inevitably leads to an overestimation of slip on the driving thrust faults, and hence of the total shortening.

Figures 9a and 9b show the effects of decompaction along regional Section 3 for the base of Calabrian horizon after removal of the lithostatic load of the Holocene and Pleistocene sediments. The measured changes in thickness with respect to the base of the Pliocene deposits range from a minimum of 10% near the structural highs (e.g. above the ramp anticline, where the Pleistocene load was minimum or absent), to a maximum of the 40% in the depocenters.

The histograms in Figure 9c show the relative variation of sedimentary load and amount of decompaction for three of our regional sections (Sections 2, 3 and 4). The histograms refer to the unload of the Pleistocene deposits from the top of the Gelasian. In all models the variation of thickness follows the same pattern, with largest variations seen in the depocenters and minimum values in the structural culminations. The average thickness change for all models is 25%. The topographic relief between anticlines and synclines is thus reduced and the remaining contrast can be attributed to genuine tectonic processes (faulting and folding).

While sediment compaction can reduce the original thickness up to 55%, the displacement losses associated with faults during sediments compaction vary between about 5% and 15% (Taylor et al., 2008). In each case, the evaluation of decompaction may be beneficial when post-faulting

burial is several kilometres and in circumstances where precise estimates of displacement, rather than general displacement trends, are required to refine fault-growth models (Taylor et al., 2008).

5.3 Fault Parallel Flow and Trishear algorithms

For faulted horizons it is appropriate to use the Fault Parallel Flow (FPF) algorithm (Egan et al., 1997; Kane et al., 1997), that was designed for kinematic modeling of the hangingwall blocks where deformation is accommodated by fault-parallel shear. The use of the trishear algorithm is instead recommended wherever the stratigraphic horizons are not offset by faults, but only warped by fault-propagation folding (Erslev, 1991; Hardy and Ford, 1997).

5.4 Dislocation modeling

We used elastic dislocation modeling to infer the geometry of the blind thrusts and the amount of fault slip needed to reproduce the shape and tectonic contrast for the folds seen in four out of seven of our shallow sections (PAa, MI, PR and FO, Figure 7). We utilized this method instead of trishear, adopted for the Sections RE, PAb, PAc (Figure 7c), because these latter sections were derived from our dataset of shallow Pleistocene horizons that did not provide any information about the geometry of the underlying thrusts, hence we had to invert the geological data to derive the fault metrics. The older horizons illustrated by these sections were either the base of the CMZs or of the ERIs (Table 1 and Figure 7). None of the horizons shown in the shallow sections are faulted.

The models we built to parameterize the active thrusts were based on standard dislocation modeling of slip on buried, rectangular faults embedded in an elastic half-space, following the theoretical formulation by Okada (1985) (Figure 7a). Although it was initially developed to model coseismic surface deformation recorded by leveling lines or GPS data, and more recently by SAR interferometry, dislocation modeling is widely used also to reconstruct fault geometries, slip rates

and earthquake recurrence from deformed geologic or geomorphic markers (e.g. Stein et al., 1988; Valensise and Ward, 1991; Ward and Valensise, 1994; Litchfield et al., 2010; Santoro et al., 2013).

As a first approximation we assumed that the shape of the folds is the average of the long-term expression of the activity of the underlying fault, thus neglecting intermediate evolutionary stages. The best fault location and geometrical parameters (length, width, minimum and maximum depth, and dip angle; see Table 2) were constrained based on a trial-and-error fit between the shape of the deformed geologic markers (i.e. the folded horizons) and the predicted displacement output of the models.

6. Slip rate calculation

In this section we present and discuss the slip rates that we calculated in this study for the selected structures (see Figure 10 and Table 3) following the procedure described in the previous section. Any temporal variations of the slip rates for the different thrust faults are shown in Figure 11. Fault displacements were always measured along the fault planes, and hence also the resulting slip rates are dip-parallel. We assumed that all structures are pure dip slip thrusts, and since the studied sections are perpendicular to the thrust systems and were designed to intersect the frontal portions of the thrust system, no component of slip outside the section trace was considered.

We paid special attention to assessing the model uncertainties. As slip rates are not independent observations but rather derived quantities, they are affected both by epistemic uncertainties and by the propagation of the errors affecting the raw data. The two basic elements in the computation of slip rates are the measure of the displacement along a specific fault and the age of a geologic marker that was offset or deformed by that fault. Although in principle this approach is quite simple, there are various sources of uncertainty affecting these quantities, some of which are not always measurable. For example, when using a seismic line as input, uncertainties may arise from the original resolution of the data acquisition, from the velocity model adopted for the depth conversion and from the procedures adopted for data interpretation. When using original raster data,

additional uncertainties may easily arise from the digitalization and georeferencing process. In our database, the younger stratigraphic data used for the shallow sections were derived from hardcopy maps where the different horizons were plotted using isobaths with a spacing of 50 m. This implies that it was impossible to resolve displacements of less than 50 m, equivalent to an average of 75 m of slip on the thrusts modeled with the Trishear or through standard elastic dislocation (Table 3). We calculated that the maximum resolution along the regional sections is 60 m, since we were forced to use raster images of interpreted seismic lines rather than original data, which implies that the minimum measurable offset is 60 m.

Following all these observations and considerations we calculated the uncertainties for each slip rate value as the sum of the individual uncertainties on the age and on the measured or derived fault slip (Table 3). In general we observe that the younger and less deformed is a horizon, the larger is the uncertainty associated with the slip rate calculation (Table 3). We compared our estimation of the uncertainties with those derived using the method proposed by Zechar and Frankel (2009) and found comparable values within the 68.27% confidence interval.

For calculating slip rates using Pleistocene horizons we were forced to adopt mean age values due to the lack of local age constraints along the sections (Table 1). This was possible also because the age uncertainties of the deformed horizons resulted in very low slip rate uncertainties, especially when compared with the uncertainties related to the estimates of total fault slip. As discussed by Haller and Basili (2011), evaluating the uncertainties in the input geological data, and hence in the slip rates derived from them, is crucial for understanding and quantifying crustal deformation and ultimately for providing reliable input for seismic hazard models.

6.1 Regional sections

6.1.1 Sections 1 and 2

The two sections image the same culminations at different structural positions, hence recording different values of total deformation (Figures 1 and 6); Section 2 shows the largest

deformation. We calculated the strain rates along Section 2 for the T2EF structure, which is the main fault-related anticline and is controlled by a system of two thrusts (Figure 6). The shallower of the two fault planes displaces the base of the Calabrian horizon by about 266 m this slip was restored using the FPF algorithm, which returned an average long-term slip rate of 0.15 mm/yr during the past 1.81 Myr. After restoring the displacement on the shallow thrust, however, the section still exhibits an anticline culmination; this structural high can be attributed to the activity of the deeper of the two thrusts, which does not offset the Calabrian deposits and that was restored using the trishear algorithm. This calculation highlighted that a further displacement of 650 m is necessary to fully restore the deformation of Calabrian deposits, which corresponds to a long-term slip rate of 0.36 mm/yr for this structure during the past 1.81 Myr. The cumulative long-term slip rate of the two thrusts is hence 0.51±0.03 mm/yr (Table 3).

The growth of the T2EF ramp anticline generated by the two faults caused the progressive erosion of most of the Pliocene succession, so that the further back-stripping of the older horizons leads to an underestimation of the true burial depths (Figure 6). A restoration of the original attitude of Gelasian and Piacenzian deposits was attempted assuming as a minimum the offset measured between the horizon cutoff on the footwall and the erosional surface cutoff on the hangingwall. The obtained slip rates of 0.56±0.08 mm/yr for the Gelasian (2.59-1.81 Myr, Table 1) and 0.25±0.06 mm/yr for the Piacenzian (3.60-2.59 Myr, Table 1) represent a minimum estimate for the activity of the fault (Table 3). The outer T3EF anticline cuts the Pliocene deposits up to the Zanclean and was restored using the trishear algorithm; this returned a long-term slip rate of 0.19±0.03 mm/yr since Calabrian times (Table 3).

Section 1 runs across the western tip of the same thrust crossed by Section 2, so the measured offsets and the deformation of Pliocene and Pleistocene horizons are significantly smaller. The T2EF structure is controlled by a single thrust (Figure 6); its restoration using the FPF algorithm yielded a long-term slip rate of 0.12±0.03 mm/yr since Calabrian times and 1.07±0.02 mm/yr for the Zanclean-Gelasian time interval.

6.1.2 Section 3

Section 3 crosses the Ferrara Thrust Front (Figure 1). We calculated slip rates for the T5FF and T6FF anticline-driving thrust faults (Figure 6 and Table 3). These two thrusts do not displace the base of the Calabrian horizon, that is deformed by fault-propagation folding. The displacement needed to restore this structure using the trishear algorithm is 830 m for the upper fault and 100 m for the deeper one, so that the long-term slip rates since Calabrian times are respectively 0.46 mm/yr and 0.06 mm/yr, resulting in a cumulative long-term slip rate of 0.52±0.03 mm/yr. For the deeper fault we managed to estimate the activity during Piacenzian and Gelasian times, using the FPF algorithm and taking into account the effects of the erosion at the hinge of the anticline. We obtained a minimum slip rate of 0.41±0.03 mm/yr.

The T6FF frontal structure of Section 3 is the leading edge of the chain in this portion of the NA outer front. We calculated the slip rate of the fault underlying this culmination using the Trishear, obtaining a long-term estimate of 0.42±0.03 mm/yr since Calabrian times.

6.1.3 Section 4

Section 4 crosses the eastern part of the Romagna Thrust Front and here we calculated the slip rate for the internal T7RF structure and for the external T9RF pop ups. The more internal thrust system (T7RF) is located onshore in the Rimini area and is formed by a set of four ramp splays connected to a deeper flat. The average orientation of this thrust system is NNW-SSE; the upper tip of the most internal and shallowest splay is at 940 m depth while that of the deepest splay is at 2,250 m depth. The internal splay dips 60° while the others become gradually more shallow-dipping. All splays connect to a single deeper flat at depth of 6,000-7,000 m. The restoration of this thrust system was performed using the Trishear algorithm by modeling a single fault having a geometry roughly coincident with that of the intermediate splays. The modeled fault has the upper tip at 4,000 m depth and dips 30° to the WSW. The resulting slip rate (1.04±0.03 mm/yr for the past

1.81 Myr) must be considered cumulative and distributed among the different splays as none of the mapped faults match exactly the modeled geometry; rather, all of them appear to contribute to the deformation of the Plio-Pleistocene horizons lying on the anticline. The T7RF turns out to be the fastest of all studied structures, in agreement with its location at the eastern end of the Northern Apennines fronts and with seismological and geodetic evidence.

We calculated the slip rates also for two adjacent pop-up anticlines located 6 km apart and belonging to the T9RF structure (Figure 6). Since all structures cut the reference horizons, we calculated the displacement cumulated during the different time intervals using the Fault Parallel Flow algorithm. The innermost pop-up has a main frontal thrust that cuts the base of the Calabrian and of the Gelasian deposits with an offset of 451 and 396 m, respectively. The associated back-thrust cuts the Gelasian deposits with a displacement of 104 m. We could measure the partitioning of activity between the frontal- and the back-thrust only for the Gelasian interval, yielding a cumulative displacement of 500 m, while there is no evidence of activity of the back-thrust during Calabrian times. The whole structure seems to have reached its maximum activity during Piacenzian times, when the fault slipped at 2.23±0.06 mm/yr. This rate decreased to 0.63±0.08 mm/yr during Gelasian times and 0.25±0.03 mm/yr since Calabrian times (Table 3). A close inspection of the outermost pop-up shows that its associated back-thrust has accommodated most of the Pleistocene deformation with a long-term slip rate of 0.11±0.03 mm/yr in the past 1.81 Myr. During Gelasian and Piacenzian times the dislocation occurred mainly along the frontal thrust with differential slip rates of 0.98±0.08 mm/yr and of 0.43±0.06 mm/yr, respectively (Table 3).

6.2 Shallow sections

6.2.1 Parma sections (PAa, PAb, PAc)

The Parma section PAa crosses the eastern termination of the Emilia Thrust Front and shows the deformation of the ERIs and ERSs horizons (Figure 7b). Their flexural folding has been reproduced using dislocation modeling of a south-dipping thrust, with a geometry similar to that

shown in the regional sections available for this area (the full geometrical parameters of the thrusts modeled along the shallow sections are listed in Table 2). The calculated slip rates are 0.30±0.19 mm/yr from the deposition of the ERSs horizon to Present and 0.40±0.18 mm/yr during the deposition of the ERIs horizon (Table 3).

A more external and deeper ramp corresponding to the frontal splay located NE of Parma in the Structural Model of Italy (Bigi et al., 1992) is imaged in section PAb. This thrust is parallel to the inner one and shares with it the same NW-SE orientation. The deformation observed in the ERIs horizon can be restored using the Trishear algorithm with a fault plane dipping 55° to the SW and having the upper tip of the slipping portion at 3,500 m depth. The resulting slip rate is 0.26±0.06 mm/yr for the past 0.82 Myr.

Section PAc represents the NW prolongation along strike of the inner splay imaged in the PAa section. The observed deformation of the base of ERIs horizon can be restored using the Trishear algorithm by modeling a fault dipping 36° and having the tip of the slipping portion of the fault at 1,900 m depth. The modeling yielded a slip rate of 0.22±0.06 mm/yr for the past 0.82 Myr. This estimate is lower than that measured for section PAa and reflects lateral variations of cumulative slip along the same fault segment. As in this case the section cuts a marginal portion of the fault, that is to say, a portion located next to the closure of the Fidenza anticline in Pliocene deposits (see Structural Model of Italy; Bigi et al., 1992), this slip rate estimate has to be taken as a minimum.

As a whole the thrust system between Fidenza and Parma appears to be more active in its southeastern part and to reduce progressively its activity toward the northwest. The slip rates obtained for these structures can be compared with the geomorphology-based estimates obtained by Ponza et al. (2010) for the Enza river valley, southeast of both the PAa and PAb structures. These investigators proposed uplift rates of 0.18 mm/yr since the end of deposition of the ERIs horizon (Figure 10 and Table 4). The slip rates calculated across the PAa section for the same time interval,

although not on the same thrust, would yield an uplift rate of 0.14±0.10 mm/yr (using the geometry of the thrust fault derived from our modeling, see Table 2).

6.2.2 Reggio Emilia section (RE)

In the Reggio Emilia section the thrust deforms the Plio-Pleistocene succession and stops its upward propagation at a depth of about 2,000 m. The deformation of the ERIs horizon was restored using the Trishear algorithm, which modeled the slip on the deeper part of the thrust yielding a slip rate of 0.10±0.06 mm/yr for the past 0.82 Myr (Table 3). The section runs orthogonally to the lateral ramp of the Ferrara arc where we expect a significant strike-slip component of fault motion: for this reason the estimate we obtained must be regarded as a minimum.

6.2.3 Mirandola section (MI)

The Mirandola anticline was investigated by Ciucci et al. (2002) and Scrocca et al. (2007) using the same dataset we used. Unlike these previous efforts, however, we used dislocation modeling to reproduce the folding of the AES7, ERSs and ERIs horizons (Figure 7b). The geometry of the thrust was constrained using the parameters of the coseismic rupture inferred from InSAR data following the 29 May 2012 earthquake (Bignami et al., 2012). The results of our calculations show that the Mirandola thrust slipped at 0.68±0.18 mm/yr during the deposition of the ERIs horizon (0.82-0.40 Myr), 0.83±0.27 mm/yr during the deposition of the ERSs and AES7 horizons (0.40-0.125 Myr), and 0.94±0.60 mm/yr during the past 0.125 Myr (Figure 11, inset in lower right corner). Taking into account the uncertainties, these estimates testify to an almost constant slip rate with an average of 0.77±0.27 mm/yr for the past 0.82 Myr.

6.2.4 Poggio Renatico section (PR)

The Poggio Renatico section crosses the central part of the Ferrara-Romagna arc. The ERIs horizon is gently folded into two short wavelength anticlines connected to two shallow splays of a

larger deep-seated thrust (Figures 5 and 7b). Dislocation modeling of the deformed horizon returned a slip rate of about 0.18 mm/yr for both splays during the past 0.82 Myr. The minimum cumulative slip rate of the deep seated thrust is 0.29±0.09 mm/yr.

6.2.5 Forlì section (FO)

The Forlì section crosses the eastern Ferrara-Romagna arc close to the Adriatic coast, and similarly to the Parma section is not far from the NA mountain front. Hence, prior to our modeling we had to take into account the original northeastward downlap depositional geometry of the silicoclastic Pleistocene succession. The ERIs horizon is gently folded due to synsedimentary activity of a thrust, that folded also the base of the Pliocene horizon (Figure 7b). For this thrust we calculated a slip rate of 0.24±0.09 mm/yr during the past 0.82 Myr.

7. Discussion

As discussed in detail in Section 3, we built our geological model of the subsurface of the Po Plain using geological and geophysical information available from the literature and from public datasets (Figure 3). As the information came from rather diverse sources, we first had to homogenize it. Then we entered it in the Move software where we reconstructed 3D models of the main subsurface horizons in a GIS-like environment (Table 1 and Figures 4 and 5). Finally, we extracted from Move a number of deep regional and shallow local sections. This workflow ensured consistency of the dataset all over the study area. We wish to stress the importance of homogenizing the input data prior to their interpretation, since they were originally obtained at different scales and for different purposes, and in many cases were derived from slightly different interpretations of the same geophysical dataset. We also wish to emphasize the importance of removing the effects of differential compaction of the sedimentary succession due to the overburden by the overlying deposits (Figures 8 and 9). Failure to give proper consideration to this step inevitably results in an overestimation of the measured fault displacements, and hence of the

inferred slip rates. Our analysis has shown an average difference of 30% between slip rates measured with and without consideration of the differential compaction effects on fault-propagation folding anticlines.

Differential compaction primarily affects the estimation of uplift rates. Scrocca et al. (2007) observed a reduction of the uplift rate of more than 50% after decompaction of Plio-Quaternary sediments along a section crossing the Mirandola anticline, and thickness changes up to the 40% of the original thickness in the depocenters due to the combined effect of decompaction and flexural isostasy. The results of our study are similar to those obtained by these investigators for the Mirandola anticline, the decompaction values being proportional to the thickness of the sedimentary layers (i.e. larger in the synclines and smaller on top of the anticlines: Figure 9b).

Our analysis of the tectonic structures (see discussion in Section 6) allowed us to build the first database of slip rates for a large portion of the southern Po Plain covering the time interval from the Pliocene to Present. The new dataset supplies estimates obtained using a common and robust workflow: from the restoration of the four regional sections we obtained slip rates for the past 3.6 Myr for seven structures, while the seven shallow sections returned slip rates for seven additional structures for the past 0.82 Myr (Table 3 and Figure 11). The slip rates contained in the database are ready to be compared with other geological strain rates (Table 4), with geodetic observations and with earthquake budgets.

The main results of our study can be summarized as follows:

1. since the youngest folded strata in our dataset are 0.125 Myr old (AES7, Tables 1 and 3), the analysis we performed allows the nature and rates of the most recent activity of the buried NA thrust fronts to be constrained much more precisely than in the recent past. We do not rule out the possibility that even younger strata are folded on top of the buried anticlines, but this deformation could not be resolved by the data we used due to the low strain rates and short time interval implied by their age. Nevertheless, ongoing activity of the NA fronts is consistent with - and in fact, proven by - the recent earthquake activity (e.g. the 2012 Emilia-Romagna sequence)

and by the control exerted on the drainage network, whose pattern highlights areas of continuous relative subsidence (i.e. the modern depocenters) and uplift (Burrato et al., 2012);

2. our differential slip rates, that is to say, the comparison of rates calculated during different time intervals, highlight a decreasing trend through time, as seen for the T2EF and T9RF structures (Figure 11, inset in lower left corner), and are in agreement with other published data (see Table 4 and references therein). This finding may explain why the activity of the buried NA fronts is still questioned by some investigators on the basis of geophysical or field evidence; it also stresses the need for incorporating high-resolution geological data in the analysis when working in slow-deforming areas such as the Po Plain, as only such data may supply details on the geometry of the most recent and shallower stratigraphic horizons;
3. our results show that over the past 1.81 Myr the cumulative slip rate of the Emilia thrust front was about 0.70 mm/yr, about 0.95 mm/yr for the Ferrara thrust front and about 1.40 mm/yr for the Romagna thrust front, following a general trend of increase towards the east (Figure 10). Such eastward increase of the cumulative strain rates agrees with the results of Boccaletti et al. (2011) and matches the GPS observations documenting an increase of shortening across the Northern Apennines fronts from about 0.5 mm/yr across the western Emilia thrust front to about 2.4 mm/yr across the Ferrara thrust front (Devoti et al., 2011; Michetti et al., 2012);
4. a similar trend is also shown by the historical earthquake record, which shows an eastward increase both in terms of the number of recorded events and in terms of total seismic moment released (Figure 1) (Burrato et al., 2004; ISIDe Working Group, 2010; Rovida et al., 2011; Vannoli et al., 2014). Since we investigated a subsample of all structures that exist in the different portions of the buried arcs, and since the missing structures could account for a significant part of the shortening budget, we cannot compare directly our data with the GPS data, that measure the total shortening across the different portions of the NA fronts;
5. our study highlighted several examples of slip partitioning between adjacent structures all along the buried arcs of the Po Plain. A good example is the T9RF structure seen along the regional

Section 4, that is formed by two pop-ups connected to the same Miocene detachment level (Figures 6 and 10, inset in lower left corner). The diagram in Figure 11 shows that the inner pop-up was characterized by higher slip rates during the Piacenzian-Gelasian interval with respect to the outer one, while during the Gelasian the outer pop-up was more active though in the framework of a general decrease of activity. Different elements may have controlled the evolution of these structures, resulting in activity phases alternating between the inner and the outer T9RF (e.g. Toscani et al., 2009). Another good example was found along Section 3, where the shallower thrust of the T5FF structure slipped at a faster rate between the Calabrian and Present, an interval during which the deeper main thrust appeared to be less active. On the contrary, the deep thrust was very active during Gelasian times, generating a fast growing anticline which led to the erosion of part of the sedimentary succession. This allowed us to estimate only a minimum for its relative slip rate;

6. the exhaustive results obtained for the Mirandola thrust allow us to make some inference on the long-term seismic behavior of the NA thrusts. The Mirandola thrust was investigated through the MI shallow section (Figure 7) and is believed to have caused the 29 May 2012, M_w 6.0 earthquake. It is one of the fastest and most documented structures included in our database, with a slip rate ranging between 0.68 and 0.94 mm/yr for the past 0.82 Myr (Figure 11). These rates appear to be almost constant or slightly increasing within the uncertainties during the time interval considered. Coseismic uplift of the anticline in 2012 was about 20 cm and the slip on the fault plane that resulted from the inversion of the SAR dataset was in the range 30-50 cm (Bignami et al., 2012; Pezzo et al., 2013). A simple calculation based on the coseismic slip and the slip rate calculated for the most recent time interval (0.94±0.60 mm/yr during the past 0.125 Myr, Table 3) yields a theoretical recharge time for 2012-type earthquakes in the range 200 to 1600 years. This wide range reflects uncertainties in the calculation of the slip rate (Table 3). However, the Italian earthquake record, that covers almost 2000 years and that for damaging earthquakes is considered complete over the past 500 years for the entire country (Stucchi et al.,

2004), does not contain any earthquake that could be even tentatively assigned to the Mirandola thrust. This observation favors a return time closer to the upper bound of the calculated time interval.

The example of the Mirandola thrust highlights a major uncertainty in the "seismic style" of the structures investigated in this work, further enhanced by the observation that in large portions of the outer NA system the contraction is accompanied by limited or no seismicity. A recent study in Italy showed that the seismic coupling *c*, a parameter first introduced for the subduction zones (Kanamori, 1971), is largely controlled by the prevalent faulting mechanism. The seismic coupling is calculated as the ratio between the seismic moment rate from earthquakes and the average moment rate expected based on geological evidence, and hence it measures how much energy actually goes into earthquake production. When averaged across areas that exhibit the same deformation style *c* turns out to be about 0.20 for Italian reverse faulting domains (Barba et al., 2010). Such a low value implies that most of the contraction is actually consumed aseismically and possibly by anelastic shear (Carafa and Barba, 2011; see also Vannoli et al., 2014).

8. Conclusions

Our 3D modeling of well dated and homogenized horizons allowed major buried fault zones of the Northern Apennines to be investigated in great detail, resulting in a new set of slip rates and associated uncertainties (Table 3).

Individual strain rates are controlled by the structural position of the investigated structures within the thrust fronts and by the geometry (i.e. the number of parallel thrusts active at the same time) of these first order tectonic elements. Variations in slip rates during the different time intervals and along the different thrust fronts show a trend of general decrease with time. Faster values are obtained along the easternmost fronts, in agreement with indications of seismic moment release and GPS-derived shortening.

The data show a major mismatch between the geological and earthquake records at the regional scale. This is hypotesized to result from poor seismic coupling, as observed also in other compressional areas in Italy and worldwide, rather than from incompleteness of the earthquake record.

Our database of slip rates includes information for only a fraction of all the buried structures of the complex NA outer fronts because the geological information included in our dataset and suitable for restoration covers only spot areas both for the regional and shallow sections. In this respect we are well aware that we documented only a fraction of the total shortening recorded along each section of the whole thrust system. Nevertheless, we believe we developed a reliable workflow that allowed us to obtain a set of slip rates in a rigorous and homogeneous fashion. We also believe our approach may be used in the future to support the seismic hazard assessment of areas that are intrinsically difficult to investigate. This approach is now ready be exported to areas characterized by flat topography and similarly slow deformation rates, or to any area where blind faulting and folding dominate; either along plate margins, such as the Los Angeles Basin (e.g. Shaw and Suppe, 1996) and the Tokyo metropolitan area (e.g. Ishiyama et al., 2013), or in intracratonic settings such as the Vienna Basin (e.g. Hinsch et al., 2005).

Acknowledgments. We wish to thank several colleagues with whom we shared discussions about various aspects of this work. In particular, we benefited from suggestions by F. C. Molinari for the Quaternary stratigraphy of the Po basin and from discussions on the active tectonics and seismic hazard of the area with the members of the DISS Working Group of INGV. We also thank G. Valensise for a thorough revision of an early version of the manuscript, and L. Jolivet Editor of the Journal, A. Lin and an anonymous Reviewer. F. E. Maesano acknowledges the support of MIUR-FIRB Project “Airplane”, code RBPR05B2ZJ. This research was partially supported by the E.C. Project GeoMol “Assessing subsurface potentials of the Alpine Foreland Basins for sustainable

planning and use of natural resources", funded by the Alpine Space Programme - European Territorial Cooperation 2007-2013.

Midland Valley is acknowledged for making available the Move software to ISPRA and University of Pavia (ASI – Academic Software Initiative).

References

Allen, P.A., Allen, J.R., 1990. Basin analysis, principles and applications. Blackwell Publishing.

Allmendinger, R.W., 1998. Inverse and forward numerical modeling of trishear fault-propagation folds. Tectonics 17 (4), 640–656, doi:10.1029/98TC01907.

Anzidei, M., Maramai, A., Montone, P. (Eds.), 2012. Special Issue on "The Emilia (northern Italy) seismic sequence of May-June, 2012: preliminary data and results". Ann. Geophys., 55 (4), 2012.

Argnani, A., Ricci Lucchi, F., 2001. Terziary siliciclastic turbidite systems of the Northern Apennines, in: Vai, G.B., Martini, I.P. (Eds.), Anatomy of an Orogen: The Apennines and Adjacent Mediterranean Basins. Springer, pp. 327–350.

Barba, S., Carafa, M.M.C., Doglioni, C. (2010). Time-independent nationwide earthquake rates derived from models and geological data. In: Barba, S., Doglioni, C. (Eds.), Project S1: Analysis of the seismic potential in Italy for the evaluation of the seismic hazard, Final Report DPC-INGV 2007-2010 S1 Project, available at: ftp://ingv.it/pro/dpcs1_dati/final_report/RUT01_deliv2_EQrate.docx.

Barba, S., Finocchio, D., Sikdar, E., Burrato, P., 2013. Modelling the interseismic deformation of a thrust system: seismogenic potential of the Southern Alps. Terra Nova 25, 221–227, doi:10.1111/ter.12026.

Basili, R., Valensise, G., Vannoli, P., Burrato, P., Fracassi, U., Mariano, S., Tiberti, M.M., Boschi, E., 2008. The Database of Individual Seismogenic Sources (DISS), version 3: Summarizing 20 years of research on Italy's earthquake geology. Tectonophysics 453, 20–43, doi:10.1016/j.tecto.2007.04.014.

Benedetti, L.C., Tapponnier, P., Gaudemer, Y., Manighetti, I., der Woerd, J., 2003. Geomorphic evidence for an emergent active thrust along the edge of the Po Plain: The Broni-Stradella fault. J. Geophys. Res. Solid Earth 108 (B5), 2238, doi:10.1029/2001JB001546.

Bennett, R.A., Serpelloni, E., Hreinsdóttir, S., Brandon, M.T., Buble, G., Basic, T., Casale, G., Cavaliere, A., Anzidei, M., Marjonovic, M., Minelli, G., Molli, G., Montanari, A., 2012. Syn-convergent extension observed using the RETREAT GPS network, northern Apennines, Italy. J. Geophys. Res. Solid Earth 117, B04408, doi:10.1029/2011JB008744.

Bertotti, G., Picotti, V., Bernoulli, D., Castellarin, A., 1993. From rifting to drifting: tectonic evolution of the South-Alpine upper crust from the Triassic to the Early Cretaceous. Sediment. Geol. 86, 53–76, doi:10.1016/0037-0738(93)90133-P.

Bigi, G., Cosentino, D., Parotto, M., Sartori, R., Scandone, P., 1990. Structural Model of Italy and Gravity Map, 1:500,000. Quad. Ric. Scientifica, 114, 3, S.EL.CA Florence.

Bignami, C., Burrato, P., Cannelli, V., Chini, M., Falcucci, E., Ferretti, A., Gori, S., Kyriakopoulos, C., Melini, D., Moro, M., Novali, F., Saroli, M., Stramondo, S., Valensise, G., Vannoli, P., 2012. Coseismic deformation pattern of the Emilia 2012 seismic sequence imaged by Radarsat-1 interferometry. Ann. Geophys. 55 (4), 789–795, doi:10.4401/ag-6157.

Boccaletti, M., Coli, M., Eva, C., Ferrari, G., Giglia, G., Lazzarotto, A., Merlanti, F., Nicolich, R., Papani, G., Postpischl, D., 1985. Considerations on the seismotectonics of the Northern Apennines. Tectonophysics 117, 7–38, doi:10.1016/0040-1951(85)90234-3.

Boccaletti, M., Corti, G., Martelli, L., 2011. Recent and active tectonics of the external zone of the Northern Apennines (Italy). Int. J. Earth Sci. (Geol. Rundsch.) 100, 1331–1348, doi:10.1007/s00531-010-0545-y.

Bonini, L., Toscani, G., Seno, S., 2014. Three-dimensional segmentation and different rupture behavior during the 2012 Emilia seismic sequence (Northern Italy). Tectonophysics, doi:http://dx.doi.org/10.1016/j.tecto.2014.05.006.

Bresciani, I., Perotti, C.R., 2014. An active deformation structure in the Po Plain (N Italy): The Romanengo anticline. Tectonics, 33, doi:10.1002/2013TC003422.

Burrato, P., Ciucci, F., Valensise, G., 2003. An inventory of river anomalies in the Po Plain, Northern Italy: evidence for active blind thrust faulting. Ann. Geophys. 46 (5), 865–882, doi:10.4401/ag-3459.

Burrato, P., Basili, R., Vannoli, P., Valensise, G., 2004. Anatomy of a thrust system from geological and seismological evidence: the case of the Northern Apennines (Italy). Eos Trans. AGU 85 (47), Fall Meet. Suppl., Abstract T14C-06.

Burrato, P., Vannoli, P., Fracassi, U., Basili, R., Valensise, G., 2012. Is blind faulting truly invisible? Tectonic-controlled drainage evolution in the epicentral area of the May 2012, Emilia-Romagna earthquake sequence (northern Italy). Ann. Geophys., 55 (4), 525–531, doi:10.4401/ag-6182.

Caporali, A., Barba, S., Carafa, M.M.C., Devoti, R., Pietrantonio, G., Riguzzi, F., 2011. Static stress drop as determined from geodetic strain rates and statistical seismicity. J. Geophys. Res. 116, B2410, doi:10.1029/2010JB007671.

Carafa, M.M.C., Barba, S., 2011. Determining rheology from deformation data: the case of central Italy. Tectonics 30, TC2003, doi:10.1029/2010TC002680.

Carafa, M.M.C., Barba, S., 2013. The stress field in Europe: optimal orientations with confidence limits. Geophys. J. Int., doi:10.1093/gji/ggt024.

Carminati, E., Doglioni, C., 2012. Alps vs. Apennines: The paradigm of a tectonically asymmetric Earth. Earth-Science Rev. 112, 67–96, doi:http://dx.doi.org/10.1016/j.earscirev.2012.02.004.

Castellarin, A., Rabbi, E., Cremonini, S., Martelli, L., Piattoni, F., 2006. New insights into the underground hydrology of the eastern Po Plain (Northern Italy). Boll. Geofis. Teor. Appl. 47 (3), 271–298.

Ciucci, F., Burrato, P., Valensise, G., 2002. Complex geomorphic response to blind thrust faulting along the northern margin of the Apennines near Mirandola (Po Plain). XXVIII General Assembly of the European Seismological Commission, Genoa, Italy 1-6 September 2002, Book of Abstracts, 203.

Cohen, K.M., Finney, S.C., Gibbard, P.L., Fan, J.-X., 2013. The ICS International Chronostratigraphic Chart. Episodes 36 (3), 199–204.

D'Agostino, N., Avallone, A., Cheloni, D., D'Anastasio, E., Mantenuto, S., Selvaggi, G., 2008. Active tectonics of the Adriatic region from GPS and earthquake slip vectors. J. Geophys. Res. Solid Earth 113, B12413, doi:10.1029/2008JB005860.

D'Anastasio, E., De Martini, P.M., Selvaggi, G., Pantosti, D., Marchioni, A., Maseroli, R., 2006. Short-term vertical velocity field in the Apennines (Italy) revealed by geodetic levelling data. Tectonophysics 418 (3–4), 219–234, doi:10.1016/j.tecto.2006.02.008.

Devoti, R., Esposito, A., Pietrantonio, G., Pisani, A.R., Riguzzi, F., 2011. Evidence of large scale deformation patterns from GPS data in the Italian subduction boundary. Earth Planet. Sci. Lett. 311 (3–4), 230–241. http://dx.doi.org/10.1016/j.epsl.2011.09.034.

Di Dio, G., Lasagna, S., Martini, A., Zanzucchi, G., 2005. Note Illustrative della Carta geologica d'Italia in scala 1:50.000, Foglio 199 Parma Sud, pp. 177, APAT.

DISS Working Group, 2010. Database of Individual Seismogenic Sources (DISS), Version 3.1.1: A compilation of potential sources for earthquakes larger than M 5.5 in Italy and surrounding areas, available at: http://diss.rm.ingv.it/diss/, © INGV 2010 - Istituto Nazionale di Geofisica e Vulcanologia - All rights reserved; doi:10.6092/INGV.IT-DISS3.1.1 (last accessed date: 29 August 2014).

Dondi, L., D'Andrea, G., 1986. La Pianura Padana e Veneta dall'Oligocene superiore al Pleistocene. Giornale di Geologia, Ser. 3, 48, 1–2, 197-225.

Egan, S.S., Buddin, T.S., Kane, S.J., Williams, G.D., 1997. Three-dimensional modelling and visualisation in structural geology: new techniques for the restoration and balancing of volumes. in: Proceedings of the 1996 Geoscience Information Group Conference on Geological Visualisation, Electronic Geology, 1, 67–82.

Erslev, E., 1991. Trishear fault-propagation folding. Geology 19 (6), 617–620, doi:10.1130/0091-7613(1991)019<0617.

Fantoni, R., Franciosi, R., 2010. Tectono-sedimentary setting of the Po Plain and Adriatic foreland. Rend. Lincei 21 (1), S197–S209, doi:10.1007/s12210-010-0102-4.

Garzanti, E., Vezzoli, G., Andò, S., 2011. Paleogeographic and paleodrainage changes during Pleistocene glaciations (Po Plain, Northern Italy). Earth-Science Rev. 105, 25–48, doi:10.1016/j.earscirev.2010.11.004.

Ghielmi, M., Minervini, M., Nini, C., Rogledi, S., Rossi, M., Vignolo, A., 2010. Sedimentary and tectonic evolution in the eastern Po-Plain and northern Adriatic Sea area from Messinian to Middle Pleistocene (Italy). Rend. Lincei 21 (1), S131–S166, doi:10.1007/s12210-010-0101-5.

Ghielmi, M., Minervini, M., Nini, C., Rogledi, S., Rossi, M., 2013. Late Miocene-Middle Pleistocene sequences in the Po Plain - Northern Adriatic Sea (Italy): The stratigraphic record of modification phases affecting a complex foreland basin. Mar. Pet. Geol. 42, 50–81, doi:10.1016/j.marpetgeo.2012.11.007.

Govoni, A., Marchetti, A., De Gori, P., Di Bona, M., Lucente, F.P., Improta, L., Chiarabba, C., Nardi, A., Margheriti, L., Agostinetti, N.P., Di Giovambattista, R., Latorre, D., Anselmi, M., Ciaccio, M.G., Moretti, M., Castellano, C., Piccinini, D., 2014. The 2012 Emilia seismic sequence (Northern Italy): Imaging the thrust fault system by accurate aftershock location. Tectonophysics 622, 44–55, doi:10.1016/j.tecto.2014.02.013.

Gunderson, K.L., Anastasio, D.J., Pazzaglia, F.J., Picotti, V., 2013. Fault slip rate variability on 104-105yr timescales for the Salsomaggiore blind thrust fault, Northern Apennines, Italy. Tectonophysics 608, 356–365, doi: http://dx.doi.org/10.1016/j.tecto.2013.09.018.

Gunderson, K.L., Pazzaglia, F.J., Picotti, V., Anastasio, D.A., Kodama, K.P., Rittenour, T., Frankel, K.F., Ponza, A., Berti, C., Negri, A., Sabbatini, A., 2014. Unraveling tectonic and climatic controls on synorogenic growth strata (Northern Apennines, Italy). Geol. Soc. Am. Bull. 126 (3–4), 532–552. doi: 10.1130/B30902.1doi:10.1130/B30902.1.

Haller, K.M., Basili, R., 2011. Developing Seismogenic Source Models Based on Geologic Fault Data. Seismol. Res. Lett. 82 (4), 519–525. doi:10.1785/gssrl.82.4.519.

Hardy, S., Ford, M., 1997. Numerical modeling of trishear fault propagation folding. Tectonics 16 (5), 841–854, doi:10.1029/97TC01171.

Heidbach, O., Tingay, M., Barth, A., Reinecker, J., Kurfeß, D., Müller, B., 2010. Global crustal stress pattern based on the World Stress Map database release 2008. Tectonophysics 482, 3–15, doi: 10.1016/j.tecto.2009.07.023.

Hinsch, R., Decker, K., Wagreich, M., 2005. 3-D mapping of segmented active faults in the southern Vienna Basin. Quat. Sci. Rev. 24, 321–336, doi:10.1016/j.quascirev.2004.04.011.

Ishiyama, T., Sato, H., Kato, N., Nakayama, T., Abe, S., 2013. Active blind thrusts beneath the Tokyo metropolitan area: Seismic hazards and inversion tectonics. Geophys. Res. Lett. 40, 2608–2612, doi:10.1002/grl.50487.

ISIDe Working Group, 2010. Italian Seismological Instrumental and parametric database, http://iside.rm.ingv.it, (last accessed date: 29 August 2014).

Kanamori, H., 1971. Great earthquakes at island arcs and the lithosphere. Tectonophysics 12, 187–198, doi:10.1016/0040-1951(71)90003-5.

Kane, S.J., Williams, G.D., Buddin, T.S., Egan, S.S., Hodgetts, D., 1997. Flexural-slip based restoration in 3D, a new approach. 1997 AAPG Annual Convention Official Program, A58.

Kastelic, V., Carafa, M., 2012. Fault slip rates for the active External Dinarides thrust-and-fold belt. Tectonics 31, TC3019, doi:10.1029/2011TC003022.

Lindquist, S.J., 1999. Petroleum systems of the Po Basin Province of Northern Italy and the Northern Adriatic Sea: Porto Garibaldi (Biogenic), Meride/Riva di Solto (Thermal), and Marnoso Arenacea (Thermal). USGS Open-File Report, 99-50-M.

Litchfield, N., Wilson, K., Berryman, K., Wallace, L., 2010. Coastal uplift mechanisms at Pakarae River mouth: Constraints from a combined Holocene fluvial and marine terrace dataset. Mar. Geol. 270, 72–83, doi:10.1016/j.margeo.2009.10.003.

Livio, F.A., Berlusconi, A., Michetti, A.M., Sileo, G., Zerboni, A., Trombino, L., Cremaschi, M., Mueller, K., Vittori, E., Carcano, C., Rogledi, S., 2009a. Active fault-related folding in the

epicentral area of the December 25, 1222 (Io=IX MCS) Brescia earthquake (Northern Italy): Seismotectonic implications. Tectonophysics 476 (1–2), 320–335, doi:10.1016/j.tecto.2009.03.019.

Livio, F., Michetti, A.M., Sileo, G., Carcano, C., Mueller, K., Rogledi, S., Serva, L., Vittori, E., Berlusconi, A., 2009b. Quaternary capable folds and seismic hazard in Lombardia (Northern Italy): the Castenedolo structure near Brescia. Ital. J. Geosci. . (Boll. Soc. Geol. It.) 128 (1), 191–200.

Maesano, F.E., Toscani, G., Burrato, P., Mirabella, F., D'Ambrogi, C., Basili, R., 2013. Deriving thrust fault slip rates from geological modeling: Examples from the Marche coastal and offshore contraction belt, Northern Apennines, Italy. Mar. Pet. Geol. 42, 122–134, doi:10.1016/j.marpetgeo.2012.10.008.

Mariotti, G., Doglioni, C., 2000. The dip of the foreland monocline in the Alps and Apennines. Earth Planet. Sci. Lett. 181, 191–202, doi:10.1016/S0012-821X(00)00192-8.

Massoli, D., Koyi, H.A., Barchi, M.R., 2006. Structural evolution of a fold and thrust belt generated by multiple décollements: analogue models and natural examples from the Northern Apennines (Italy). J. Struct. Geol. 28, 185–199, doi:10.1016/j.jsg.2005.11.002.

Michetti, A.M., Giardina, F., Livio, F., Mueller, K., Serva, L., Sileo, G., Vittori, E., Devoti, R., Riguzzi, F., Carcano, C., Rogledi, S., Bonadeo, L., Brunamonte, F., Fioraso, G., 2013. Active compressional tectonics, Quaternary capable faults, and the seismic landscape of the Po Plain (northern Italy). Ann. Geophys. 55 (5), 969–1001, doi:10.4401/ag-5462.

Montone, P., Mariucci, M.T., 1999. Active stress along the NE external margin of the Apennines: the Ferrara arc, northern Italy. J. Geodyn. 28, 251–265, doi:10.1016/S0264-3707(98)00041-6.

Montone, P., Mariucci, M.T., Pierdominici, S., 2012. The Italian present-day stress map. Geophys. J. Int. 189, 705–716, doi:10.1111/j.1365-246X.2012.05391.x.

Muttoni, G., Carcano, C., Garzanti, E., Ghielmi, M., Piccin, A., Pini, R., Rogledi, S., Sciunnach, D., 2003. Onset of major Pleistocene glaciations in the Alps. Geol. 31 , 989–992. doi:10.1130/G19445.1

MPS Working Group, 2004. Redazione della mappa di pericolosità sismica prevista dall'Ordinanza PCM 3274 del 20 marzo 2003. Final report for the Department of Civil Protection, INGV, Milan, April 2004, 65 pp. + 5 Appendices, http://zonesismiche.mi.ingv.it.

Muttoni, G., Carcano, C., Garzanti, E., Ghielmi, M., Piccin, A., Pini, R., Rogledi, S., Sciunnach, D., 2003. Onset of major Pleistocene glaciations in the Alps. Geology, 31 (11), 989-992, doi:10.1130/G19445.1.

Muttoni, G., Scardia, G., Kent, D. V., Morsiani, E., Tremolada, F., Cremaschi, M., Peretto, C., 2011. First dated human occupation of Italy at ~0.85 Ma during the late Early Pleistocene climate transition. Earth Planet. Sci. Lett. 307 (3–4), 241–252, doi:10.1016/j.epsl.2011.05.025.

Okada, Y., 1985. Surface deformation due to shear and tensile faults in a half-space. Bull. Seismol. Soc. Am. 75 (4), 1135–1154.

Pezzo, G., Merryman Boncori, J.P., Tolomei, C., Salvi, S., Atzori, S., Antonioli, A., Trasatti, E., Novali, F., Serpelloni, E., Candela, L., Giuliani, R., 2013. Coseismic Deformation and Source Modeling of the May 2012 Emilia (Northern Italy) Earthquakes. Seismol. Res. Lett. 84 (4), 645–655, doi:10.1785/0220120171.

Picotti, V., Pazzaglia, F.J., 2008. A new active tectonic model for the construction of the Northern Apennines mountain front near Bologna (Italy). J. Geophys. Res. 113, B08412, doi:10.1029/2007JB005307.

Pondrelli, S., Salimbeni, S., Ekström, G., Morelli, A., Gasperini, P., Vannucci, G., 2006. The Italian CMT dataset from 1977 to the present. Phys. Earth Planet. Inter. 159 (3–4), 286–303, doi:10.1016/j.pepi.2006.07.008.

Pondrelli, S., Salimbeni, S., Morelli, A., Ekström, G., Postpischl, L., Vannucci, G., Boschi, E., 2011. European–Mediterranean Regional Centroid Moment Tensor catalog: Solutions for 2005–2008. Phys. Earth Planet. Inter. 185 (3–4), 74–81, doi:10.1016/j.pepi.2011.01.007.

Pondrelli, S., Salimbeni, S., Perfetti, P., Danecek, P., 2012. Quick regional centroid moment tensor solutions for the Emilia 2012 (northern Italy) seismic sequence. Ann. Geophys. 55 (4), 615–621, doi:10.4401/ag-6146.

Ponza, A., Pazzaglia, F.J., Picotti, V., 2010. Thrust-fold activity at the mountain front of the Northern Apennines (Italy) from quantitative landscape analysis. Geomorphology 123 (3–4), 211–231, doi:10.1016/j.geomorph.2010.06.008.

Quigley, M., Villamor, P., Furlong, K., Beavan, J., Van Dissen, R., Litchfield, N., Stahl, T., Duffy, B., Bilderback, E., Noble, D., Barrell, D., Jongens, R., Cox, S., 2010. Previously Unknown Fault Shakes New Zealand's South Island. Eos, Trans. Am. Geophys. Union 91 (49), 469–470, doi:10.1029/2010EO490001.

Ravaglia, A., Seno, S., Toscani, G., Fantoni, R., 2006. Mesozoic extension controlling the Southern Alps thrust front geometry under the Po Plain, Italy: Insights from sandbox models. J. Struct. Geol. 28, 2084–2096, doi:10.1016/j.jsg.2006.07.011.

Regione Emilia-Romagna (R.E.R.) and ENI-AGIP, 1998. Riserve idriche sotterranee nella Regione Emilia-Romagna. Di Dio, G. (Ed.), 119 pp., 9 sheets, S.EL.CA., Firenze.

Regione Lombardia (R.L.) and ENI-AGIP, 2002. Geologia degli Acquiferi Padani della Regione Lombardia. Carcano, C., Piccin, A. (Eds.), 130 pp., 9 sheets, S.EL.CA., Firenze.

Rovida A., Camassi, R., Gasperini, P., Stucchi, M. (Eds.), 2011. CPTI11, the 2011 version of the Parametric Catalogue of Italian Earthquakes. Milano, Bologna, http://emidius.mi.ingv.it/CPTI, (last accessed date: 29 August 2014).

Santoro, E., Ferranti, L., Burrato, P., Mazzella, M.E., Monaco, C., 2013. Deformed Pleistocene marine terraces along the Ionian Sea margin of southern Italy: Unveiling blind fault-related folds contribution to coastal uplift. Tectonics 32, 737–762, doi:10.1002/tect.20036.

Scardia, G., De Franco, R., Muttoni, G., Rogledi, S., Caielli, G., Carcano, C., Sciunnach, D., Piccin, A., 2012. Stratigraphic evidence of a Middle Pleistocene climate-driven flexural uplift in the Alps. Tectonics 31, TC6004, doi:10.1029/2012TC003108.

Sclater, J.G., Christie, P.A.F., 1980. Continental stretching: An explanation of the Post-Mid-Cretaceous subsidence of the central North Sea Basin. J. Geophys. Res. Solid Earth 85, 3711–3739, doi:10.1029/JB085iB07p03711.

Scognamiglio, L., Margheriti, L., Mele, F.M., Tinti, E., Bono, A., Gori, P. De, Lauciani, V., Lucente, F.P., Mandiello, A.G., Marcocci, C., Mazza, S., Pintore, S., Quintiliani, M., 2012. The 2012 Pianura Padana Emiliana seimic sequence: locations, moment tensors and magnitudes. Ann. Geophys. 55 (4), 549–559, doi:10.4401/ag-6159.

Scrocca, D., Carminati, E., Doglioni, C., Marcantoni, D., 2007. Slab Retreat and Active Shortening along the Central-Northern Apennines, in: Lacombe, O., Roure, F., Lavé, J., Vergés, J. (Eds.), Thrust Belts and Foreland Basins SE - 25, Frontiers in Earth Sciences. Springer Berlin Heidelberg, pp. 471–487, doi:10.1007/978-3-540-69426-7_25.

Serpelloni, E., Anzidei, M., Baldi, P., Casula, G., Galvani, A., 2005. Crustal velocity and strain-rate fields in Italy and surrounding regions: new results from the analysis of permanent and non-permanent GPS networks. Geophys. J. Int. 161, 861–880, doi:10.1111/j.1365-246X.2005.02618.x.

Serpelloni, E., Vannucci, G., Pondrelli, S., Argnani, A., Casula, G., Anzidei, M., Baldi, P., Gasperini, P., 2007. Kinematics of the Western Africa-Eurasia plate boundary from focal mechanisms and GPS data. Geophys. J. Int. 169, 1180–1200, doi:10.1111/j.1365-246X.2007.03367.x.

Servizio Geologico d'Italia, 2002. Geological Map of Italy, 1:50,000 scale, Sheet 223 Ravenna.

Servizio Geologico d'Italia - APAT, 2005a. Geological Map of Italy, 1:50,000 scale, Sheet 199 Parma Sud.

Servizio Geologico d'Italia - APAT, 2005b. Geological Map of Italy, 1:50,000 scale, Sheet 240-241 Forlì-Cervia.

Servizio Geologico d'Italia - ISPRA, 2009a. Geological Map of Italy, 1:50,000 scale, Sheet 181 Parma Nord.

Servizio Geologico d'Italia - ISPRA (2009b), Geological Map of Italy, 1:50,000 scale, Sheet 203 Poggio Renatico.

Shaw, J.H., Suppe, J., 1996. Earthquake hazards of active blind-thrust faults under the central Los Angeles basin, California. J. Geophys. Res. Solid Earth 101, 8623–8642, doi:10.1029/95JB03453.

Sileo, G., Giardina, F., Livio, F., Michetti, A.M., Mueller, K., Vittori, E., 2007. Remarks on the Quaternary tectonics of the Insubria region (Lombardia, NW Italy), and Ticino, SE Switzerland). Ital. J. Geosci. (Boll. della Soc. Geol. Ital.) 126 (2), 411–425.

Stein, R.S., King, G.C.P., Rundle, J.B., 1988. The Growth of Geological Structures by Repeated Earthquakes 2. Field Examples of Continental Dip-Slip Faults. J. Geophys. Res. 93 (B11), 13319–13331, doi:10.1029/JB093iB11p13319.

Stein, R., Yeats, R.S., 1989. Hidden Earthquakes. Sci. Am., 260, 48-57.

Stramondo, S., Saroli, M., Tolomei, C., Moro, M., Doumaz, F., Pesci, A., Loddo, F., Baldi, P., Boschi, E., 2007. Surface movements in Bologna (Po Plain — Italy) detected by multitemporal DInSAR. Remote Sens. Environ. 110, 304–316, doi:10.1016/j.rse.2007.02.023.

Stucchi, M., Albini, P., Mirto, M., Rebez, A., 2004. Assessing the completeness of Italian historical earthquake data. Ann. Geophys. 47 (2–3), 659–673, doi:10.4401/ag-3330.

Taylor, S.K., Nicol, A., Walsh, J.J., 2008. Displacement loss on growth faults due to sediment compaction. J. Struct. Geol. 30, 394–405, doi:10.1016/j.jsg.2007.11.006.

Teatini, P., Tosi, L., Strozzi, T., 2011. Quantitative evidence that compaction of Holocene sediments drives the present land subsidence of the Po Delta, Italy. J. Geophys. Res. 116, B08407, doi:10.1029/2010JB008122.

Toda, S., Awata, Y., 2008. Does the 2007 Noto Hanto earthquake reveal a weakness in the Japanese national seismic hazard map that could be remedied with geological data? Earth, Planets Sp. 60 (10), 1047–1052, doi:10.1186/BF03352867.

Toscani, G., Seno, S., Fantoni, R., Rogledi, S., 2006. Geometry and timing of deformation inside a structural arc; the case of the western Emilian folds (Northern Apennine front, Italy). Boll. della Soc. Geol. Ital. 125 (1), 59–65.

Toscani, G., Burrato, P., Di Bucci, D., Seno, S., Valensise, G., 2009. Plio-Quaternary tectonic evolution of the Northern Apennines thrust fronts (Bologna-Ferrara section, Italy): seismotectonic implications. Ital. J. Geosci. (Boll. della Soc. Geol. Ital.) 128 (2), 605–613, doi:10.3301/IJG.2009.128.2.605.

Valensise, G., Ward, S.N., 1991. Long-term uplift of the Santa Cruz coastline in response to repeated earthquakes along the San Andreas fault. Bull. Seismol. Soc. Am. 81, 1694–1704.

Vannoli, P., Basili, R., Valensise, G., 2004. New geomorphic evidence for anticlinal growth driven by blind-thrust faulting along the northern Marche coastal belt (central Italy). J. Seismol. 8, 297–312, doi:10.1023/B:JOSE.0000038456.00574.e3.

Vannoli, P., Burrato, P., Valensise, G., 2014. The seismotectonics of the Po Plain (northern Italy): tectonic diversity in a blind faulting domain. Pure Appl. Geophys., doi:10.1007/s00024-014-0873-0.

Ward, S.N., Valensise, G., 1994. The Palos Verdes terraces, California: Bathtub rings from a buried reverse fault. J. Geophys. Res. Solid Earth 99 (B3), 4485–4494, doi:10.1029/93JB03362.

Wegmann, K.W., Pazzaglia, F.J., 2009. Late Quaternary fluvial terraces of the Romagna and Marche Apennines, Italy: Climatic, lithologic, and tectonic controls on terrace genesis in an active orogen. Quat. Sci. Rev. 28, 137–165, doi:10.1016/j.quascirev.2008.10.006.

Zechar, J.D., Frankel, K.L., 2009. Incorporating and reporting uncertainties in fault slip rates. J. Geophys. Res. Solid Earth 114, B12407, doi:10.1029/2009JB006325.

Zehnder, A.T., Allmendinger, R.W., 2000. Velocity field for the trishear model. J. Struct. Geol. 22, 1009–1014, doi:10.1016/S0191-8141(00)00037-7.

Tables

Table 1. Timescale and regional key stratigraphic units

Epoch	Stage	Unit		Age of the base of horizon (Myr)	Sedimentary environment
Holocene		Ravenna subsynthem	AES8	0.015	Continental
Pleistocene	Upper	Villa Verrucchio subsynthem	AES7	0.125	
	Middle	Emiliano-Romagnolo Superiore synthem	ERS_s	0.40 (0.35-0.45)	
		Emiliano-Romagnolo Inferiore synthem	ERI_s	0.82 (0.78-0.87)	
	Calabrian	Costamezzana synthem	CMZ_s	1.0 (0.94-1.07)	Marine
				1.81	
	Gelasian			2.59	
Pliocene	Piacenzian			3.60	
	Zanclean			5.33	
Miocene	Messinian			7.25	

Table 1: Timescale and regional key stratigraphic units used in this work. The ages in Myr indicated for these units are those defined for their base by previous investigators (see reference in the text) and may not exactly correspond to the ages as given by Cohen et al. (2013).

Table 2. Geometrical parameters of individual thrusts from dislocation modeling

id	Section	Fault System	Strike (°)	Dip (°)	Rake (°)	Length (km)	Width (km)	Min depth (km)	Max depth (km)
1	PA	EF	132	40	90	8.0	5.5	1.0	4.5
2	RE	FF	38	40	90	6.4	4.7	4.0	7.0
3	MI	FF	108	30	90	9.0	5.9	4.0	7.0
4	PR	FF	91	40	90	3.6	3.1	1.0	3.0
5	PR	FF	103	45	90	3.6	3.1	1.0	3.2
6	FO	RF	123	40	90	8.0	5.5	3.0	6.5

Table 2: Geometrical parameters of the thrusts derived from dislocation modeling and used to calculate the slip rates along the shallow sections. Fault systems: EF, Emilia Thrust Front; FF, Ferrara Thrust Front; RF, Romagna Thrust Front.

Table 3. Slip rates calculated in this study

Section	Structure	Lat. N	Lon. E	Age interval Myr (min-max)		Total slip m	Slip rate mm/yr	Uncertainty mm/yr	Relative uncertainties	Method	DISS source	Notes
1	T2EF	45.215	9.598	0	1.81	212	0.12	0.03	28%	FPF	ITCS044	
1	T2EF	45.215	9.598	1.81	5.3	3751	1.07	0.02	2%	FPF	ITCS044	
2	T2EF	45.179	9.718	0	1.81	916	0.51	0.03	7%	FPF-TR	ITCS044	cumulative of deep and shallow thrusts
2	T2EF	45.179	9.718	1.81	2.59	450	0.56	0.08	13%	TR	ITCS044	minimum due to erosion
2	T2EF	45.179	9.718	2.59	3.6	253	0.25	0.06	24%	FPF	ITCS044	minimum due to erosion
2	T3EF	45.285	9.777	0	1.81	340	0.19	0.03	18%	TR	n.a.	
3	T5FF	44.703	11.794	0	1.81	930	0.52	0.03	6%	TR	ITCS012	cumulative
3	T5FF	44.703	11.794	1.81	3.6	729	0.41	0.03	8%	FPF	ITCS012	deep thrust; minimum due to erosion
3	T6FF	44.833	11.875	0	1.81	750	0.42	0.03	8%	TR	ITCS050	
4	T7RF	44.127	12.338	0	1.81	1875	1.04	0.03	3%	TR	ITCS039	cumulative of different splays
4	T9RF in	44.366	12.628	0	1.81	451	0.25	0.03	13%	FPF	n.a.	frontal thrust
4	T9RF in	44.366	12.628	1.81	2.59	500	0.63	0.08	12%	FPF	n.a.	cumulative of back- and frontal thrusts
4	T9RF in	44.366	12.628	2.59	3.6	2227	2.23	0.06	3%	FPF	n.a.	
4	T9RF out	44.412	12.680	0	1.81	205	0.11	0.03	29%	FPF	n.a.	back-thrust
4	T9RF out	44.412	12.680	1.81	2.59	786	0.98	0.08	8%	FPF	n.a.	frontal thrust
4	T9RF out	44.412	12.680	2.59	3.6	434	0.43	0.06	14%	FPF	n.a.	frontal thrust
PAa	PAa	44.776	10.239	0	0.4	121	0.30	0.19	62%	DM	ITCS009	ERSs
PAa	PAa	44.776	10.239	0.4	0.82	167	0.40	0.18	45%	DM	ITCS009	ERIs-ERSs
PAa	PAa	44.776	10.239	0	0.82	288	0.35	0.18	52%	DM	ITCS009	cumulative
PAb	PAb	44.841	10.331	0	0.82	214	0.26	0.06	23%	TR	ITCS009	
PAc	PAc	44.907	10.065	0	0.82	180	0.22	0.06	28%	TR	ITCS009	
RE	RE	44.781	10.575	0	0.82	81	0.10	0.06	62%	TR	ITCS049	ERIs
MI	MI	44.864	11.077	0	0.125	118	0.94	0.60	64%	DM	ITCS051	AES7
MI	MI	44.864	11.0767	0.125	0.4	227	0.83	0.27	33%	DM	ITCS051	ERSs-AES7
MI	MI	44.864	11.077	0	0.4	345	0.86	0.38	43%	DM	ITCS051	cumulative
MI	MI	44.864	11.077	0.4	0.82	287	0.68	0.18	66%	DM	ITCS051	ERIs-ERSs
MI	MI	44.864	11.077	0	0.82	632	0.77	0.27	36%	DM	ITCS051	cumulative
PR	PR	44.695	11.587	0	0.82	235	0.29	0.09	32%	DM	ITCS012	ERIs
FO	FO	44.278	12.094	0	0.82	200	0.24	0.09	38%	DM	ITCS011	ERIs

Table 3: Slip rates calculated in this study. Method: FPF, Fault Parallel Flow; TR, trishear; DM, dislocation modeling. The column DISS refers to the Id number of the Composite Seismogenic Sources of the DISS database (DISS Working Group, 2010) to which the analyzed structures can be ascribed.

Table 4. Slip rates and uplift rates in the Po basin from literature data

Id	Lat. N	Lon. E	Age interval Myr (min-max)		D-SR mm/yr	R-SR mm/yr	UR mm/yr	Fault system	Name	Ref.
1	45.188	9.629	0	1.81	----	1.50	----	EF	Casalpusterlengo	a
2	45.188	9.629	1.81	5.30	----	1.40	----	EF	Casalpusterlengo	a
3	44.871	10.889	0	1.8	----	0.80	----	FF	Novellara	a
4	44.871	10.899	1.81	5.30	----	7.20	----	FF	Novellara	a
5	44.910	11.671	0	1.81	----	1.50	----	FF	Ferrara	a
6	44.910	11.670	1.81	5.30	----	6.10	----	FF	Ferrara	a
7	44.662	12.049	0	1.81	----	0.60	----	FF	Comacchio	a
8	44.662	12.049	1.81	5.30	----	5.00	----	FF	Comacchio	a
9	44.840	11.135	0	0.125	----	----	0.16	FF	Mirandola	b
10	44.840	11.135	0.125	0.40	----	----	0.26	FF	Mirandola	b
11	44.840	11.135	0.40	0.65	----	----	0.33	FF	Mirandola	b
12	44.840	11.135	0.65	1.40	----	----	0.53	FF	Mirandola	b
13	45.080	9.376	0	0.015	----	----	0.30	EF	Stradella	c
14	44.507	10.947	0	0.23	----	----	0.29	PTF	Castelvetro	d
15	44.669	10.506	0	0.40	----	----	0.18	PTF	Ghiardo	d
16	45.473	10.125	1.20	1.60	----	2.69	----	SA	Capriano del Colle	e
17	45.473	10.125	0.90	1.20	----	2.75	----	SA	Capriano del Colle	e
18	45.473	10.125	0	0.90	----	0.43	----	SA	Capriano del Colle	e
19	45.468	10.285	0	0.90	----	0.10	----	SA	Castenedolo	e
20	45.468	10.285	0.90	1.20	----	----	0.00	SA	Castenedolo	e
21	45.468	10.285	1.20	1.60	----	----	0.13	SA	Castenedolo	e
22	45.323	10.328	0	0.90	----	0.04	0.03	SA	Manerbio	f
23	45.323	10.328	1.20	1.60	----	0.76	0.51	SA	Manerbio	f
24	45.809	8.897	0	0.90	----	----	0.11	SA	Monte Morone	g
25	45.837	8.981	0	5.30	----	----	0.04	SA	Novazzano	g
26	45.802	9.166	0	0.78	----	----	0.27	SA	Albese con Cassano	g
27	45.468	10.285	0	0.89	0.4	----	----	SA	Castenedolo	h
28	45.473	10.125	0	0.89	0.5	----	----	SA	Capriano del Colle	h

29	43.920	12.816	0	0.125	----	0.24-0.36	----	MCB	Pesaro	i
30	43.616	13.327	0	2.59/3.60	----	0.52-0.37	----	MCB	Pesaro-Senigallia	l
31	43.669	13.428	0	2.20/2.59	----	1.35-1.14	----	MCB	Conero onshore N	l
32	43.696	13.598	0	3.00/3.60	----	0.58-0.49	----	MCB	Conero offshore N	l
33	43.566	13.591	0	2.20/2.59	----	1.20-1.01	----	MCB	Conero onshore S	l
34	43.595	13.690	0	3.00/3.60	----	0.91-.76	----	MCB	Conero offshore S	l
35	43.633	13.851	0	3.60/5.30	----	0.54-0.37	----	MCB	Colosseo	l
36	43.822	13.912	0	3.60/5.30	----	0.38-0.26	----	MCB	Clara 1	l
37	44.845	9.9831	0	1.81	0.3	----	----	PTF	Salsomaggiore	m
38	44.845	9.9831	1.81	2.00	2.7	----	----	PTF	Salsomaggiore	m
39	44.845	9.9831	2.00	2.59	0.6	----	----	PTF	Salsomaggiore	m
40	44.845	9.9831	2.59	3.00	1.4	----	----	PTF	Salsomaggiore	m
41	45.397	9.810	0	0.87	----	----	0.17-0.07	SA	Romanengo	n
42	45.397	9.810	1.80	2.58	----	----	0.173-0.163	SA	Romanengo	n
43	45.397	9.810	2.58	3.60	----	----	0.39-0.27	SA	Romanengo	n
44	45.397	9.810	3.60	5.33	----	----	0.246-0.249	SA	Romanengo	n

Table 4: Dip parallel (D-SR), Rake parallel (R-SR) slip rates and uplift rates (UR) along the Northern Apennines and Southern Alps thrust fronts in the Po Plain basin and surrounding areas, taken from literature data. Fault systems: EF, Emilia Thrust Front; FF, Ferrara Thrust Front; MCB, Marche Coastal Belt; PTF, Pedeapenninic Thrust Front; RF, Romagna Thrust Front; SA, Southern Alps thrust front. Key to references: a, Boccaletti et al. (2011); b, Scrocca et al. (2007); c, Benedetti et al. (2003); d, Ponza et al. (2010); e, Livio et al. (2009a); f, Livio et al. (2009b); g, Sileo et al. (2007); h, Michetti et al. (2012); i, Vannoli et al. (2004); l, Maesano et al. (2013); m, Gunderson et al. (2013); n, Bresciani and Perotti (2014). Notice that the data are inhomogeneous both for the age intervals and the type of slip measured (uplift rate, dip parallel, or rake parallel).

Figure captions

Figure 1. Schematic structural and seismotectonic map of the Po basin and location of the studied cross-sections. Thrust fronts and fault systems are shown with thick grey lines. Contour of the base of the Plio-Quaternary sediments are shown with thin grey lines (modified from Structural Model of Italy, Bigi et al., 1992). Surface anticlines: CA, Castanedolo; CC, Capriano al Colle; CV, Castelvetrano; GH, Ghiardo; MO, Montello; SC, San Colombano; SM, Salsomaggiore; TV, Trino Vercellese. Regional cross sections (shown in Figure 6): 1, 2, 3 and 4. Shallow sections (shown in Figure 7): PAa, PAb and PAc, Parma sections; RE, Reggio Emilia; MI, Mirandola; PR, Poggio Renatico; FO, Forlì. Instrumental seismicity of $M \geq 3.5$ in the 2005-2013 interval is shown by circles of size proportional to the magnitude (ISIDe Working Group, 2010); the epicenters of the 20 and 29 May 2012 earthquakes are shown as stars (A and B, respectively). Historical seismicity of $M \geq 5.5$ from CPTI11 Catalogue is shown by squares of size proportional to the magnitude (Rovida et al., 2011). Focal mechanisms and P axes of the two largest shocks of the 2012 Emilia-Romagna earthquake sequence are from Scognamiglio et al. (2012); others from the RCMT Catalog (http://www.bo.ingv.it/RCMT/); P axes are represented as white bars. Thin grey bars are Shmax axes from Carafa and Barba (2013). Grey arrows are GPS vectors from Caporali et al. (2011).

Figure 2. Simplified Meso-Cenozoic tectono-stratigraphic scheme of the Po Plain (modified after Fantoni and Franciosi, 2010), showing also the main detachment levels. Synthems subdivision according to Regione Emilia Romagna and ENI-AGIP, 1998; Regione Lombardia and ENI-AGIP, 2002; Servizio Geologico d'Italia, 2002; 2005a, b; 2009a, b). * indicates upper Messinian sediments. The vertical scale does not match exactly the duration of each Period and Epoch.

Figure 3. Dataset used for this study. Keys: the grey lines show subsurface data and interpreted seismic lines; the grey rectangles show the areas covered by subsurface data from the sheets of the Geological Map of Italy (1:50,000 scale). Key: A, Sheet 181 Parma nord (Servizio Geologico

d'Italia - ISPRA, 2009a); B, Sheet 199 Parma sud (Servizio Geologico d'Italia - APAT, 2005a); C, Sheet 203 Poggio renatico (Servizio Geologico d'Italia - ISPRA, 2009b); D, Sheet 223 Ravenna (Servizio Geologico d'Italia, 2002); E and F, Sheets 240-241 Forlì-Cervia (Servizio Geologico d'Italia - APAT, 2005b). Other subsurface data used are the Pliocene isobaths (blue dashed boundary; Bigi et al., 1992) and the three main aquifers of the Po Plain: Aquifer A (grey boundary); Aquifer B (yellow boundary) and Aquifer C (light blue boundary) (Regione Emilia-Romagna and ENI-AGIP, 1998; Regione Lombardia and ENI-AGIP, 2002).

Figure 4. 3D surface of the base of the Plio-Quaternary deposits in map view (isobaths after Structural Model of Italy, Bigi et al., 1992). Red lines, traces of the regional sections; pink lines, traces of the shallow sections.

Figure 5. 3D surface of the base of the Emiliano-Romagnolo Inferiore Synthem (ERIs; 0.65-0.80 Myr) in map view (Table 1). Isobaths after Regione Emilia-Romagna and ENI-AGIP (1998) and Regione Lombardia and ENI-AGIP (2002). Red lines, regional sections; pink lines, shallow sections. A, area for which more detailed data are available from the Sheet 203 - Poggio Renatico of the Geological Map of Italy (Servizio Geologico d'Italia - ISPRA, 2009b); B, 3D surface generated using the most detailed data and showing syncline-anticline couples along the PR shallow section (pink line is the section trace, white line is the intersection with the ERIs surface).

Figure 6. Regional sections crossing the Emilia, Ferrara and Romagna thrust fronts (traces in Figure 1). All sections are 80 km long and show the whole NA buried chain and the SA fronts (Sections 1 and 2) and the foreland of the Ferrara and Romagna fronts (Sections 3 and 4). Section 1, modified after Toscani et al. (2006); Sections 2, 3 and 4, modified after Fantoni and Franciosi (2010). The colors of the different units are the same as in Figure 2. The Quaternary units are not

visible at this scale. The structures have been numbered as in the text. LT, Ligurian thrust; PTF, Pedeapenninic Thrust Front. No vertical exaggeration.

Figure 7. a) Shallow sections derived from the 3D model; the horizons AES8, AES7, ERSs, ERIs, CMZs and the base of Pliocene deposits are represented with different vertical scales (grey areas indicates the changes of vertical scale). b) Interpreted seismic lines: PR-399-91 (PAb), PR-387-90 (Pac), and RE-383-91 (RE) (ViDEPI Project, available from http://unmig.sviluppoeconomico.gov.it/videpi/). Black dashed lines highlight growth strata and fold geometries. c) Location map of the shallow sections and geometry of fault planes used for dislocation modeling and Thrishear.

Figure 8. Workflow and methods adopted for restoration and slip-rate calculations.

Figure 9. Effects of the decompaction on the slip rate calculation. a) Comparison of the 3D model derived from the regional Section 3 before and after the decompaction of the Gelasian deposits due to removal of overlying units. The topographic relief is reduced after unloading; the depth marker in the corner of the model indicates a rebound ranging from about 1,600 m to about 950 m. b) A portion of the regional Section 3 is shown to highlight the relationships between the thickness changes after removal of the Pleistocene-Holocene sediment burden (shown as arrows of variable size) and the position of the tectonic structures (i.e. depocenters and structural culminations). c) The diagrams show the relationship between the thickness of the sedimentary load (blue line) (e.g. the Pleistocene succession) and the amount of decompaction (red bars) along the regional Sections 2, 3 and 4. Notice that the effect of decompaction is smaller above of structural highs, where the thickness of intervening deposits is smaller.

Figure 10. Location of the slip rates calculated in this work shown as green squares and labeled as in Table 3. With the blue circles are shown the slip rate and uplift rate data available from the literature and labeled as in Table 4.

Figure 11. Synthesis of the results of the slip rate calculation for regional and shallow sections and for different time intervals. The size of the circles is proportional to the slip rate; each symbol is labeled with the Id of the relevant structure (same as in Table 3 and in text). The diagrams in the lower part of the figure show the evolution of activity of the T9RF structure along the regional Section 4 (left), and of the Mirandola thrust along the shallow section MI (right).

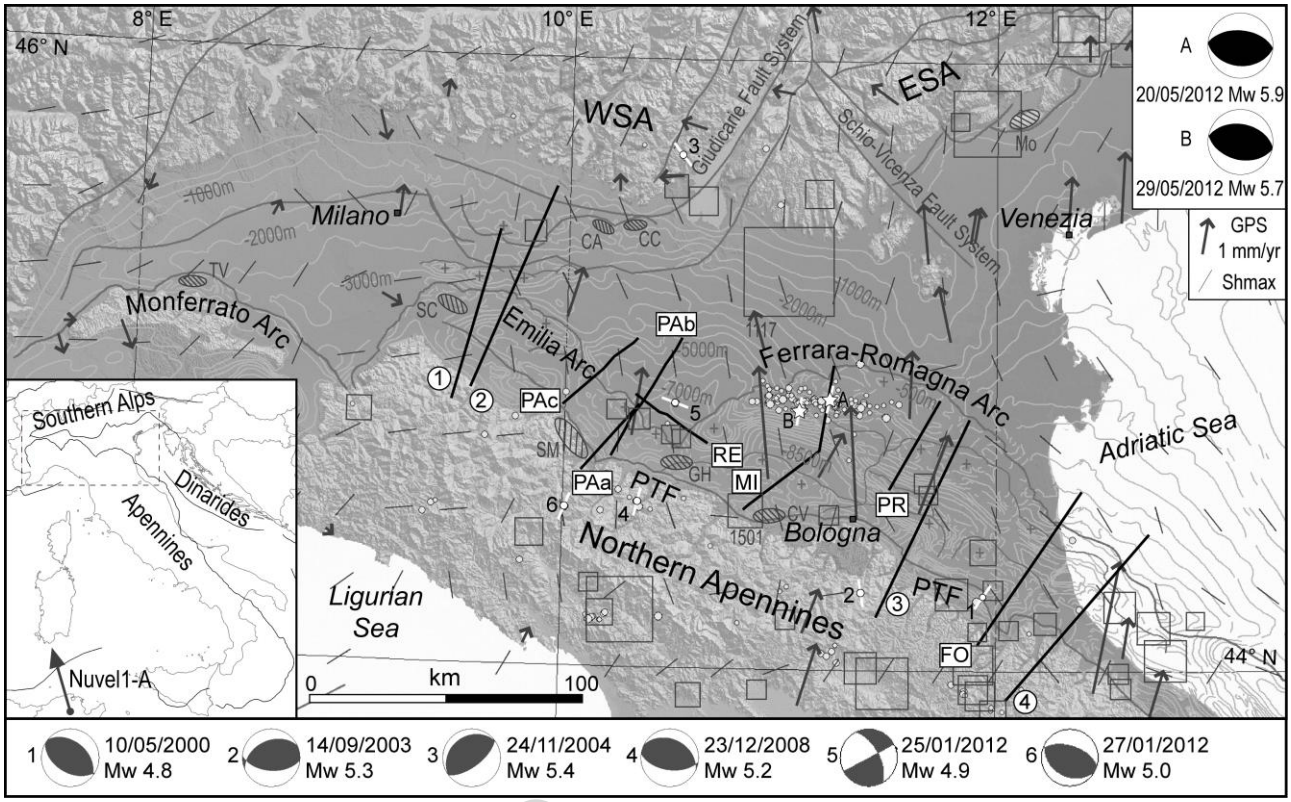

Fig. 1

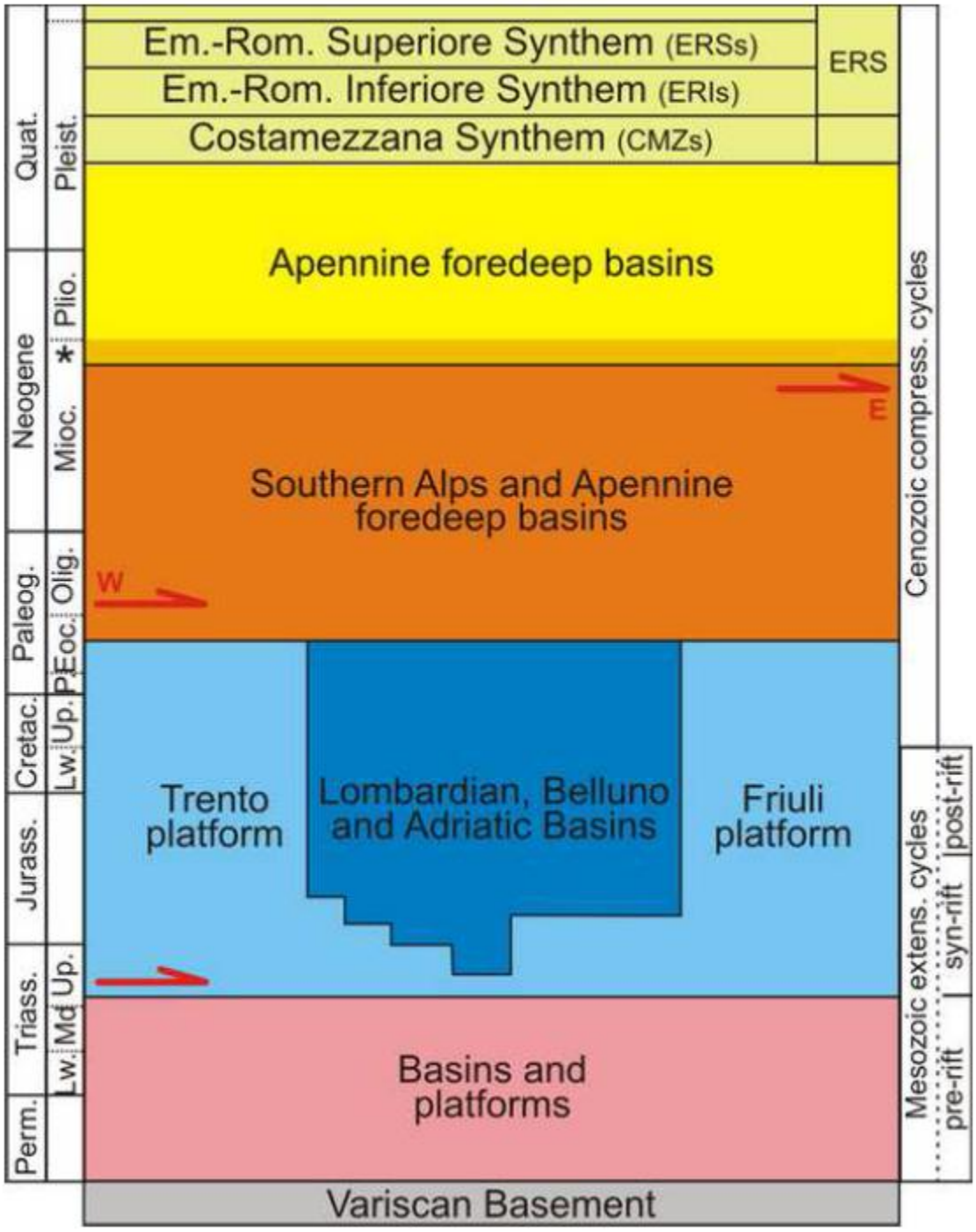
Em.-Rom. Superiore Synthem (ERSs)
Em.-Rom. Inferiore Synthem (ERIs)
Costamezzana Synthem (CMZs)
ERS
Apennine foredeep basins
Southern Alps and Apennine foredeep basins
E
W
Trento platform
Lombardian, Belluno and Adriatic Basins
Friuli platform
Basins and platforms
Variscan Basement
Cenozoic compress. cycles
Mesozoic extens. cycles
post-rift
syn-rift
pre-rift
Quat.
Pleist.
Neogene
Plio.
Mioc.
Paleog.
Olig.
Eoc.
Cretac.
Up.
Lw.
Jurass.
Triass.
Md
Up.
Lw.
Perm.

Fig. 2

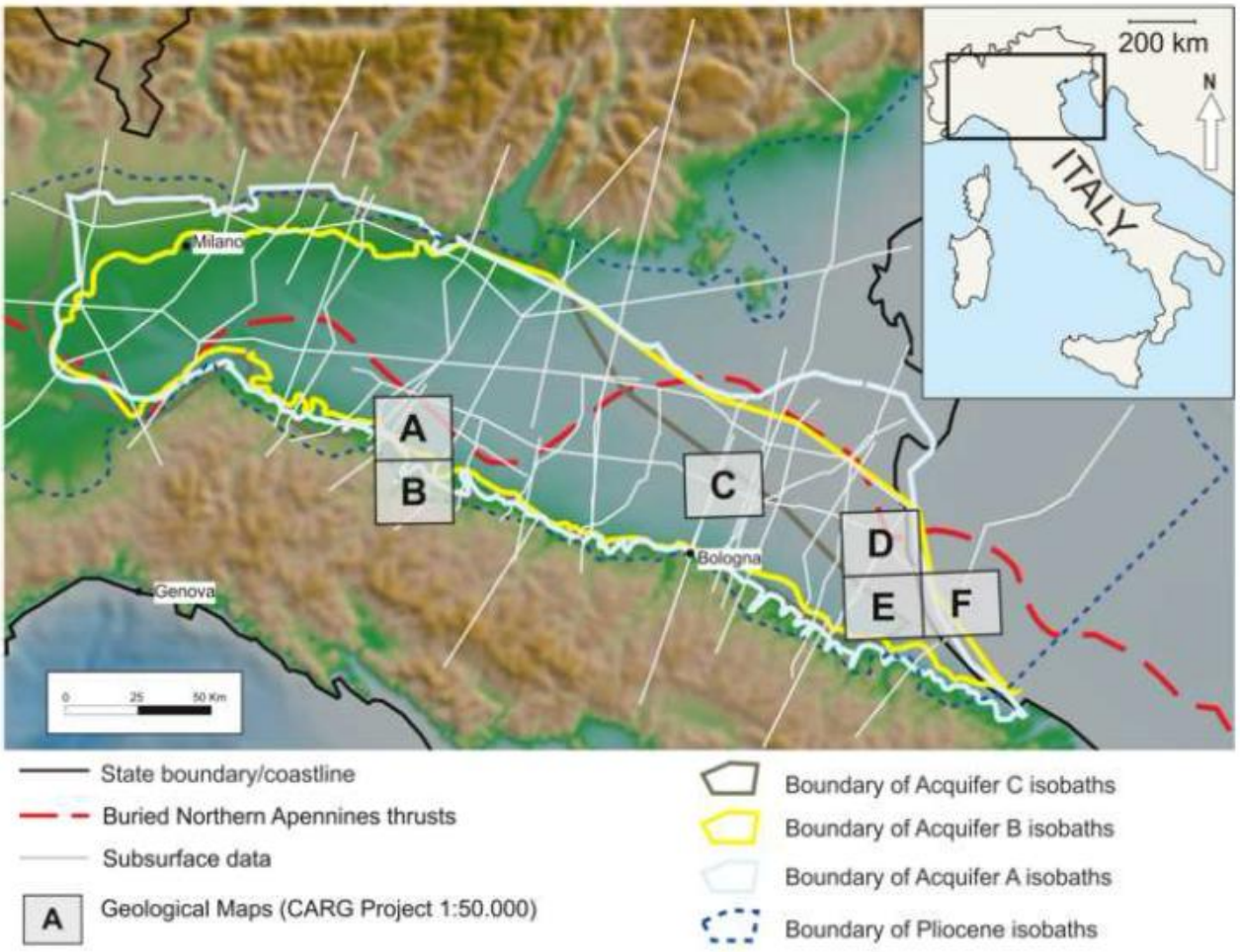

Fig. 3

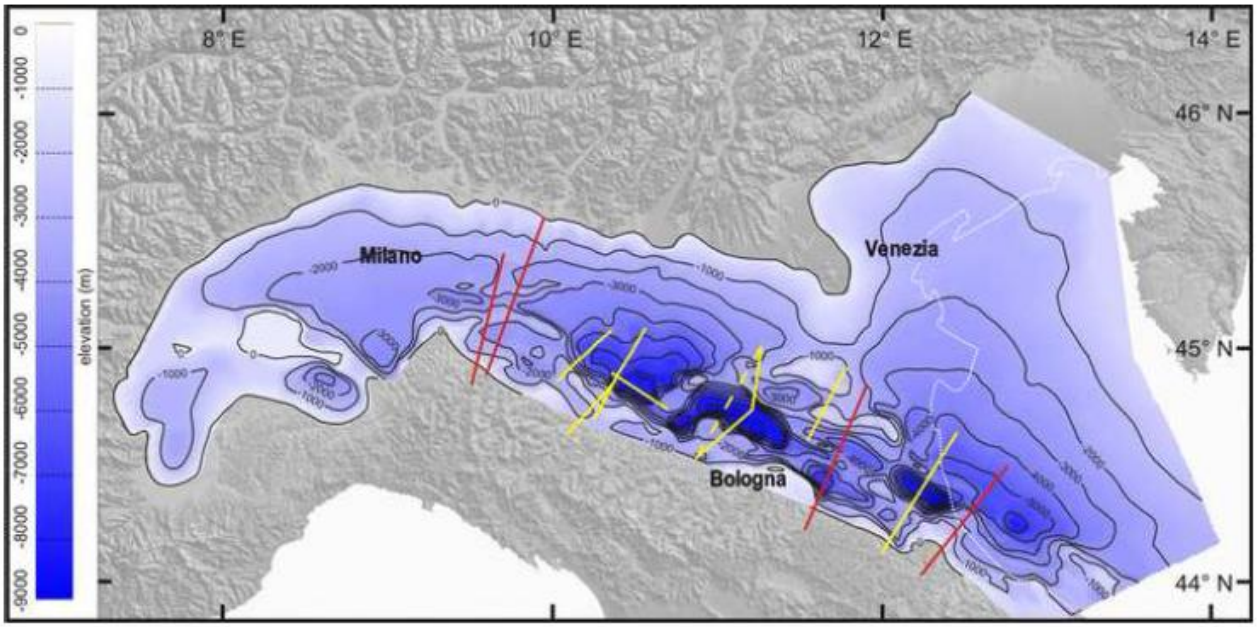

Fig. 4

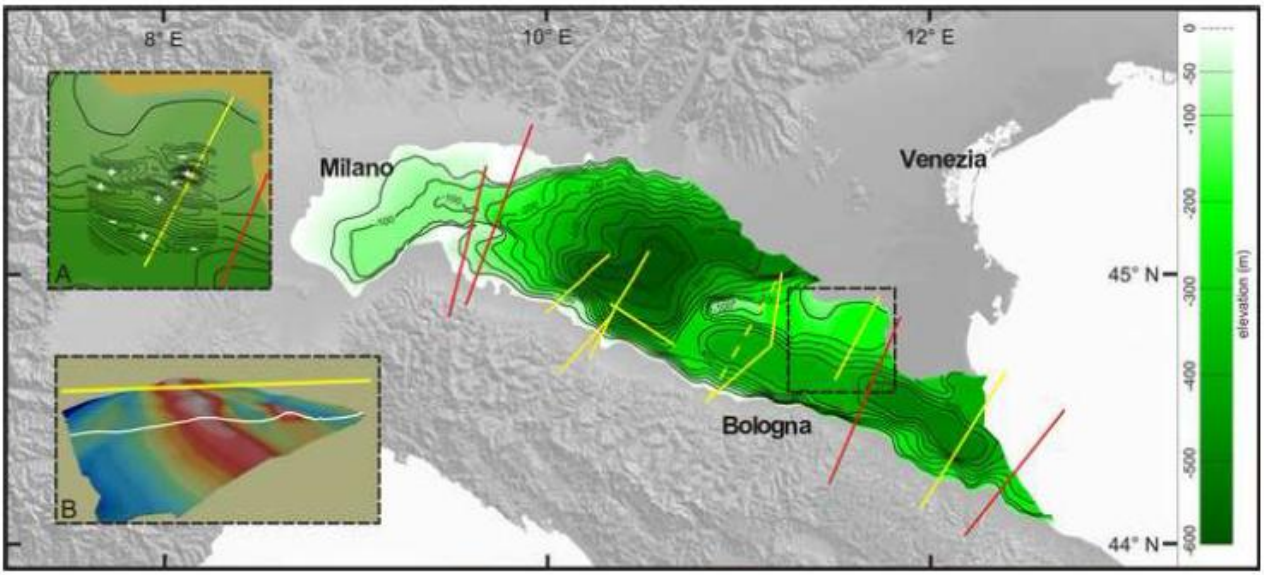

Fig. 5

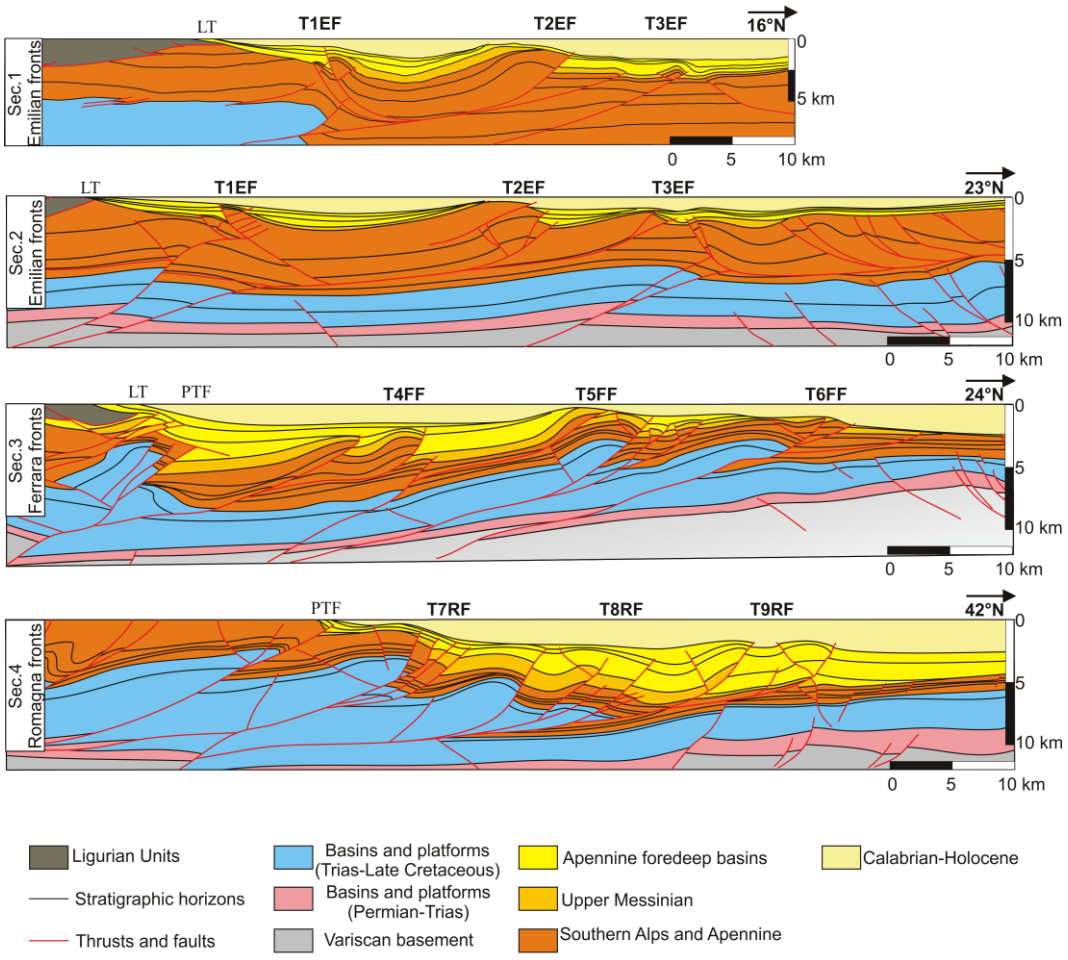

Fig. 6

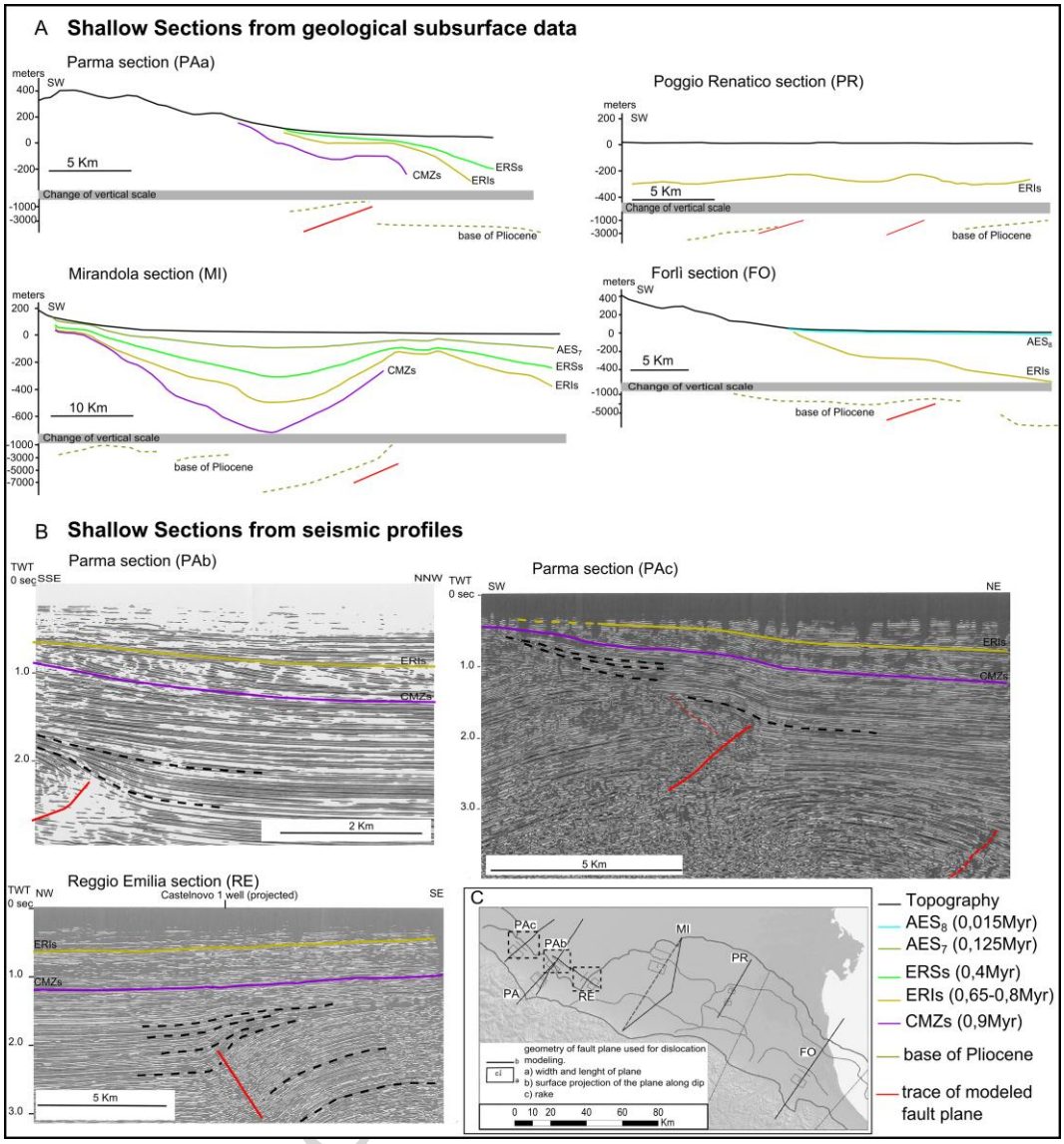

Fig. 7

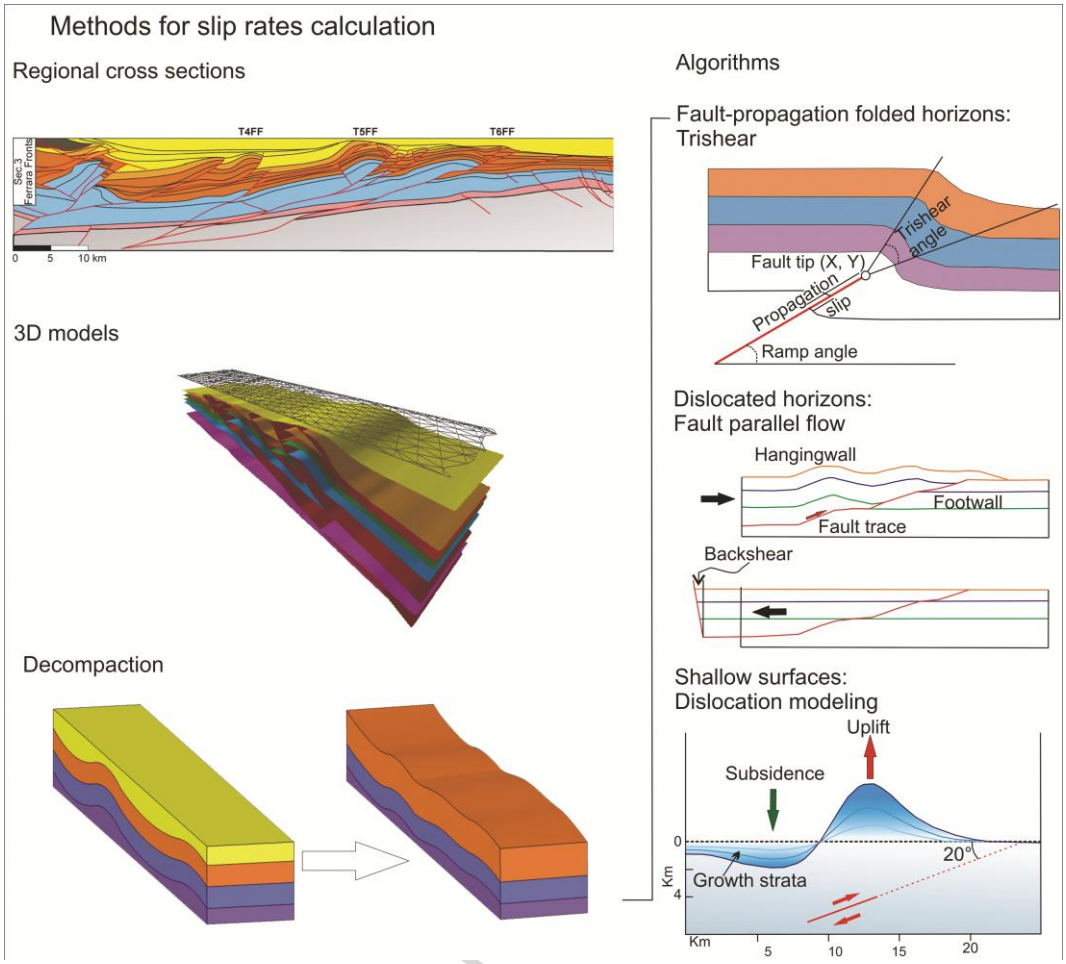
Methods for slip rates calculation
Regional cross sections
T4FF
T5FF
T6FF
Sec-3
Terzia Fronts
0
5
10 km
3D models
Decompaction
Algorithms
Fault-propagation folded horizons:
Trishear
Trishear angle
Fault tip (X, Y)
Propagation
slip
Ramp angle
Dislocated horizons:
Fault parallel flow
Hangingwall
Footwall
Fault trace
Backshear
Shallow surfaces:
Dislocation modeling
Uplift
Subsidence
0
Km
4
Growth strata
20°
Km
5
10
15
20

Fig. 8

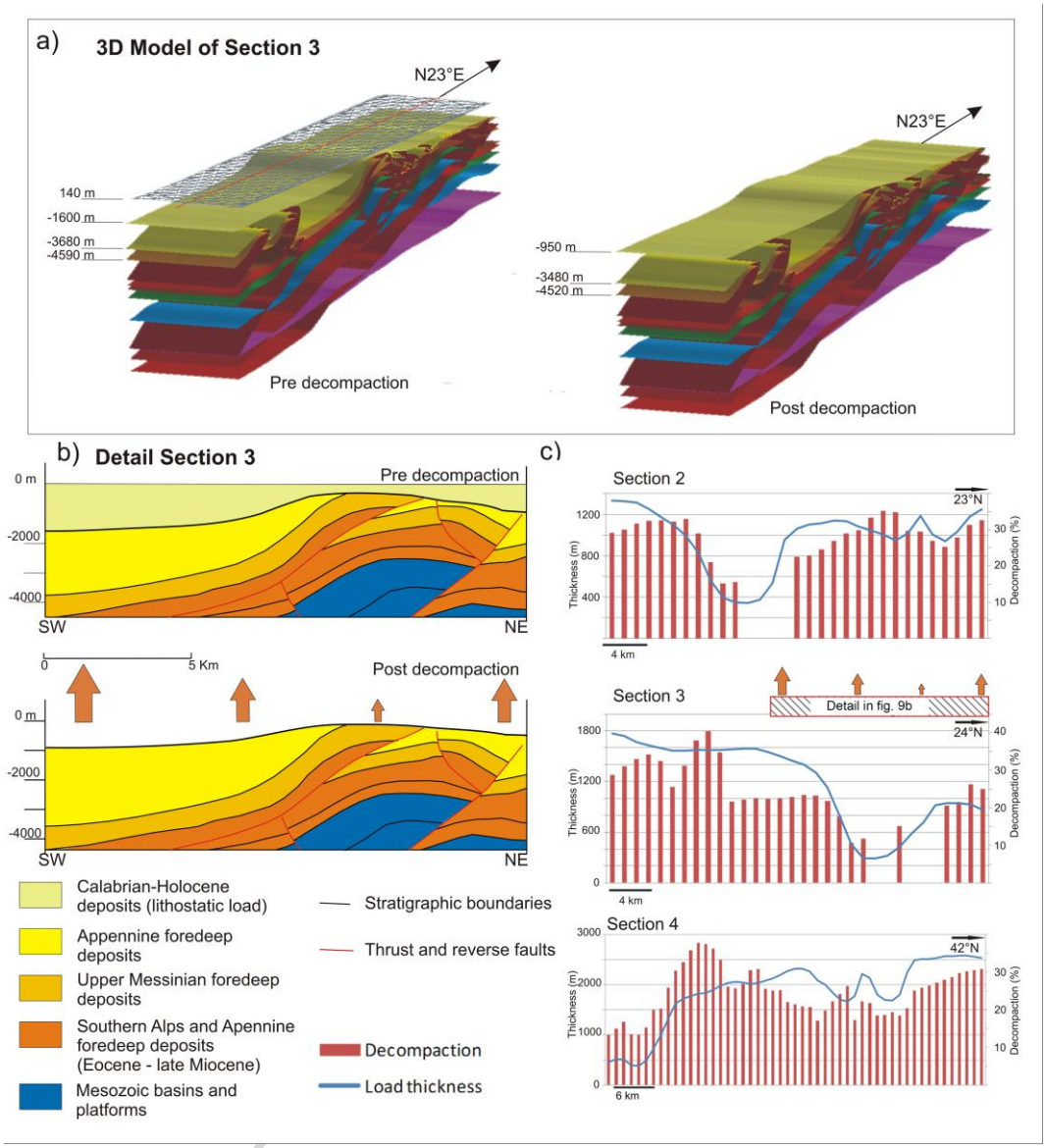

Fig. 9

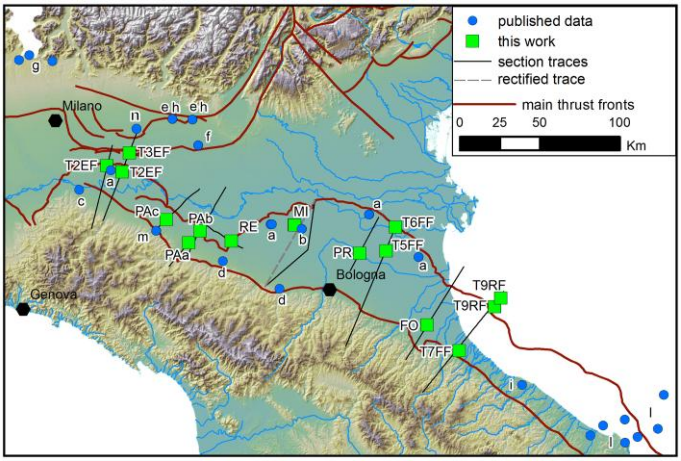

Fig. 10

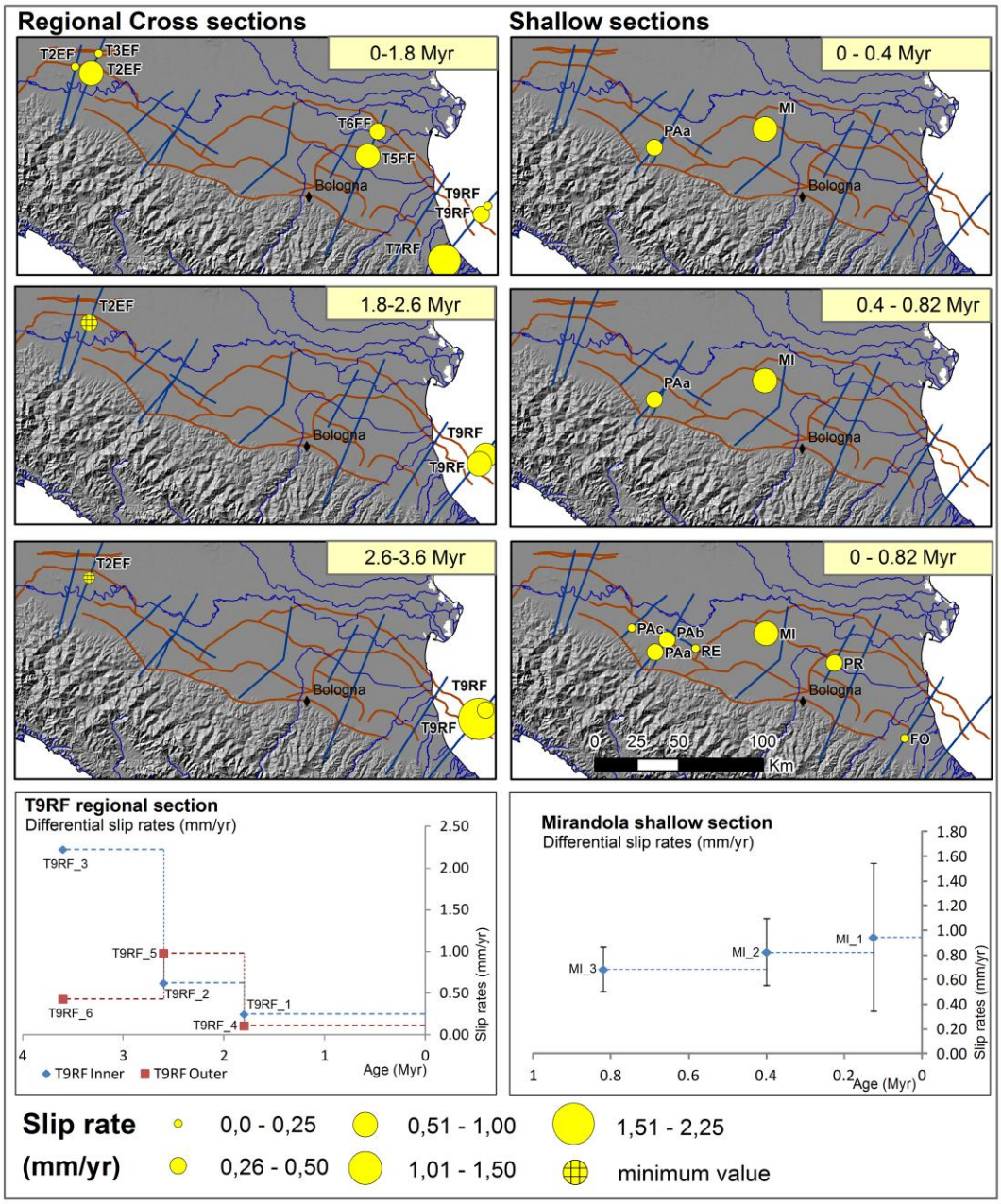
Regional Cross sections
Shallow sections
0-1.8 Myr
0 - 0.4 Myr
1.8-2.6 Myr
0.4 - 0.82 Myr
2.6-3.6 Myr
0 - 0.82 Myr
T2EF
T3EF
T6FF
T5FF
T9RF
T7RF
MI
PAa
PAc
PAb
RE
PR
FO
Bologna
0
25
50
100
Km
T9RF regional section
Differential slip rates (mm/yr)
T9RF_3
T9RF_5
T9RF_2
T9RF_1
T9RF_6
T9RF_4
T9RF Inner
T9RF Outer
Age (Myr)
Slip rates (mm/yr)
Mirandola shallow section
Differential slip rates (mm/yr)
MI_3
MI_2
MI_1
Slip rate
(mm/yr)
0,0 - 0,25
0,26 - 0,50
0,51 - 1,00
1,01 - 1,50
1,51 - 2,25
minimum value

Fig. 11

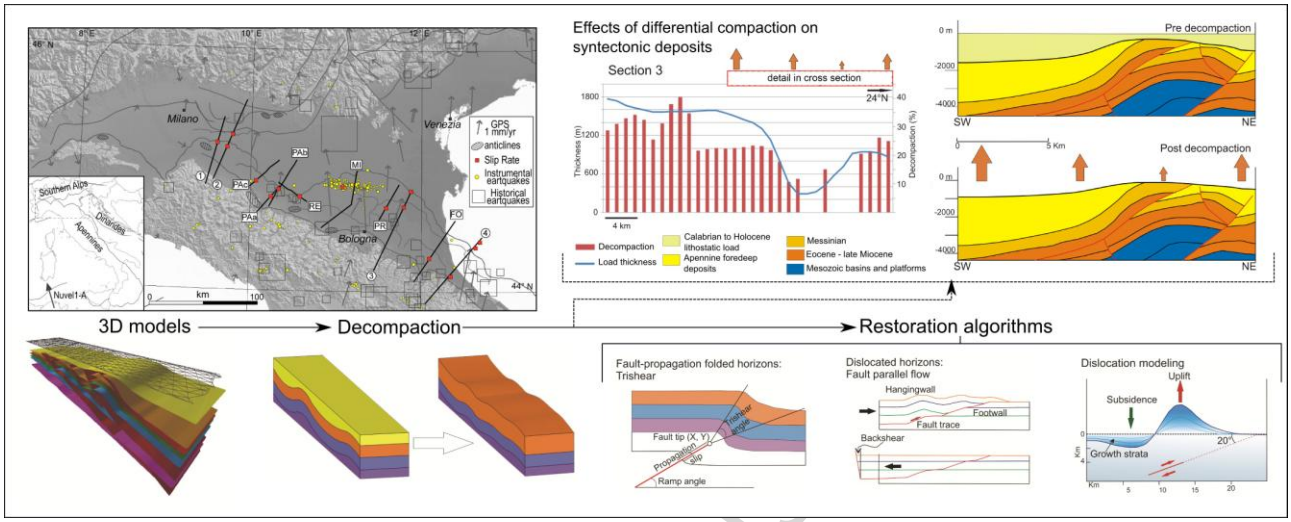

Graphical abstract

Highlights

- We calculated 28 slip rate values on 14 blind thrusts in the Po Plain
- Slip rates range between 0.1-1 mm/yr during last 1.81 Myr
- The Mirandola thrust slipped at 0.86±0.38 mm/yr during the last 0.4 Myr
- Youngest identified folded strata in our dataset are 0.125 Myr old
- Decompacting using 3D models helps resolving fault activity in sedimentary basins